Endonucleolytic RNA cleavage drives changes in gene expression during the innate immune response

Agnes Karasik[1], Hernan A. Lorenzi[2], Andrew V. DePass[1] and Nicholas R. Guydosh[1]

[1]Laboratory of Biochemistry and Genetics, National Institute of Diabetes and Digestive and Kidney Diseases, National Institutes of Health, Bethesda, MD 20892

[2]TriLab Bioinformatics Group, National Institute of Diabetes and Digestive and Kidney Diseases, National Institutes of Health, Bethesda, MD 20892

Keywords: RNase L, RNase A, endonuclease, Integrated Stress Response, ZAKα, ribosome collisions

Highlights:

- Activated RNase L acts with dsRNA-sensing pathways to promote cell signaling
- RNA fragmentation induces transcription through ZAKα signaling
- Activation of RNase L modulates levels of eIF2α phosphorylation
- Translation of the *GADD34* and *IFIT* mRNAs is inhibited by active RNase L

Summary

Viral infection triggers several dsRNA sensors that lead to changes in gene expression in the cell. One of these sensors activates an endonuclease, RNase L, that cleaves single stranded RNA. However, how the resultant widespread RNA fragmentation affects gene expression is not fully understood. Here we show that this fragmentation induces the Ribotoxic Stress Response via ZAKα, potentially through ribosome collisions. The p38 and JNK pathways that are activated as part of this response promote outcomes that inhibit the virus, such as programmed cell death. We also show that RNase L limits the translation of stress-responsive genes, including antiviral *IFIT* mRNAs and *GADD34* that encodes an antagonist of the Integrated Stress Response. Intriguingly, we found the activity of the generic endonuclease, RNase A, recapitulates many of the same molecular phenotypes as activated RNase L, demonstrating how widespread RNA cleavage can evoke an antiviral program.

Introduction

Viral infections are recognized by Pattern Recognition Receptors (PRRs) that trigger the innate immune response and ultimately promote elimination of pathogens. Foreign nucleic acid (RNA or DNA) sensing is one of the major ways viral pathogens are recognized [1]. Viruses have either an RNA genome or produce RNA intermediates, and thus sensing of viral RNA in the cytoplasm is vital for recognizing and fighting against viruses. A subset of PRRs recognize double stranded RNA (dsRNA) [1]. One group within these PRRs is the interferon-induced family of Oligo-Adenylate Synthetases (OAS1-3) that produce an oligomer of adenylates chained together through 2'-5' linkages (2-5A) upon dsRNA binding. 2-5A can selectively bind Ribonuclease L (RNase L) to induce dimerization that is required for its transition from a latent to an activated state. Activated RNase L then cleaves a variety of host and viral RNAs, triggering many downstream processes and physiological changes in the cell. These changes include the loss of most mRNAs (and therefore gene expression in the cell), production of chemokines and cytokines, activation of inflammasomes, inhibition of cell migration, autophagy, senescence, and cell death [2-5]. Intriguingly, the function of RNase L appears to extend beyond its role in protecting against viruses. RNase L mutations increase risk for multiple types of cancer, including prostate and breast cancer [6-9], and autoimmune diseases [10].

Besides RNase L, another interferon-regulated PRR, Protein Kinase R (PKR), can induce reduction in protein synthesis in the cell through phosphorylation of eukaryotic Initiation Factor 2α (eIF2α). Phospho-eIF2α inhibits initiation of translation of the majority of mRNAs, presumably to limit viral protein production, and triggers a number of changes in the cell that are collectively referred to as the Integrated Stress Response (ISR) [11-13]. Additionally, the dsRNA receptors RIG-I and MDA5 induce the interferon and inflammatory response by activating signaling that leads to transcription. Activation of the different dsRNA response pathways in the cytoplasm can have intersecting functions, wherby activated RIG-I induces gene expression, while activated RNase L and PKR reduce gene expression. However, how the different dsRNA sensing pathways, particularly RNase L, act together to achieve a strong antiviral response is largely unknown.

67 Activation of RNase L can induce and alter transcription [14-17]. During RNase L
68 activation, many proinflammatory genes and cytokines (e.g. CXCL8) were found to be
69 upregulated in early microarray studies [14]. Importantly, more recent RNA-sequencing
70 (RNA-seq) studies found that most transcripts are degraded (~60 to >99%) by RNase L.
71 Interestingly, immune transcripts, such as interferon-β (IFNβ), are able to compensate for
72 this degradation via transcriptional upregulation or resistance to cleavage due to
73 underrepresentation of favorable RNase L cleavage motifs (UU or UA) [16,17]. Furthermore,
74 many Interferon Stimulated Genes (ISGs) are upregulated during the dsRNA response in
75 both WT and *RNASEL* KO cells, suggesting that they do not depend on RNase L,
76 whereas upregulation of cytokines, such as CXCL8, CXCL2, and other immune genes,
77 including *IFNL1* and *2*, and *IFIT3*, were at least partially dependent on RNase L [17]. These
78 observations suggest that active RNase L together with the other dsRNA pathways may
79 amplify transcription of antiviral genes. In some cell lines, RNase-L cleaved RNA
80 fragments play a role in activating RIG-I [18,19] and the inflammasome [20], however interferon
81 stimulation (downstream of RIG-I) was not observed in human lung carcinoma cells
82 [16,17,21]. One limitation of the existing studies that used RNA-seq is that RNase L was
83 activated by a dsRNA mimic (poly I:C), an approach that simultaneously activates many
84 other pathways [16,17]. These pathways can mask RNase L-specific effects and make it
85 difficult to assess how RNase L activation and the other dsRNA pathways act together to
86 induce the antiviral immune response.
87 Importantly, activation of RNase L can also induce pathways related to the
88 Ribotoxic Stress Response (RSR) [22,23], which triggers apoptosis through transcription
89 activated by JNK (c-JUN N-terminal Kinase) signaling, which is a mitogen-activated
90 protein kinase (MAPK) family member. While several MAP2K family members can
91 phosphorylate JNK [23], the mechanism of how they are activated by RNase L has
92 remained unclear. The RSR was originally shown to be activated by defective translation,
93 so it was suggested that pathways related to the RSR were induced when RNase L
94 damaged ribosomes by cleaving rRNA [22-24]. However, more recently, it was revealed that
95 ribosomes with cleaved rRNAs are functional, suggesting that ribosome damage may not
96 be responsible for activating the RSR [16]. In addition, the RSR was recently shown to
97 include activation of the MAP3K family member ZAKα that senses collisions between

98 ribosomes and phosphorylates MAP2Ks that, in turn, phosphorylate JNK, and another
99 MAPK, p38 [25-28]. These observations suggest that activation of ZAKα by ribosome
100 collisions could occur when RNase L induces the RSR. However, the source of any
101 potential ribosome collisions in RNase L activated cells remains unknown. One possible
102 source of ribosome collisions was suggested by our previous observation that activation
103 of RNase L leads to translation of fragmented mRNAs [21]. Ribosomes that translate mRNA
104 fragments would have the possibility of reaching a 3' end without terminating, an event
105 known to lead to ribosome stalling and the formation of ribosome collisions [29].
106 More broadly, the overall loss of translated mRNA in the cell upon RNase L
107 activation is expected to change the balance of free ribosomal subunits and mRNAs [16].
108 This altered balance could modulate the translation efficiency of the remaining, full-length
109 transcripts. Consistent with this, we previously observed an increase in the relative
110 proportion of ribosomes in alternative Open Reading Frames (ORFs) or "altORFs"
111 following RNase L activation [21]. We proposed that translation of these altORFs became
112 more favorable as excess free ribosomes promoted translation initiation at the 5' ends of
113 the RNA fragments created by RNase L. However, how RNase L and other dsRNA
114 pathways lead to changes in translation on mRNAs remained unclear.
115 Here we investigated how direct activation of RNase L, and attendant global mRNA
116 degradation, contributes to the activation of the innate immune response. We found that
117 RNase-L mediated RNA cleavage strengthened multiple parts of the antiviral
118 transcriptional response and, in particular, induced ZAKα activation, presumably via
119 ribosome collisions. In addition, activation of RNase L also changed how efficiently intact
120 mRNAs were translated, in some cases by inhibiting the effect of eIF2α phosphorylation.
121 Our results highlight the multifaceted role of RNase L and endonucleolytic cleavage in
122 promoting antiviral functions.
123
124 **Results**
125
126 **Activation of RNase L induces transcription and phosphorylation of ZAKα**
127 To measure changes in the transcriptome under activation of RNase L, but not
128 other components of the dsRNA-induced innate immune response, we performed RNA-

129 seq on wild type (WT) and *RNASEL* KO cells that were transfected with 2-5A (1 μM), the
130 direct and specific activator of RNase L (Figure 1A). Since RNase L cleaves rRNA, we
131 utilized a rRNA degradation assay to assess the level of RNase L activation [30]. Across all
132 our replicates, we found that rRNA degradation was similar (within a 2-fold difference,
133 Figure S1A). Based on previous reports that used spike-in oligos for normalization [16,17],
134 these levels of rRNA degradation correspond to a loss of ~60% to >99% of individual
135 mRNAs in the cell. We therefore assume that the absolute abundance of most mRNAs in
136 the treated cells under study here substantially decreases ("baseline loss").
137 Then, we analyzed differential expression (DE) patterns in 2-5A treated vs
138 untreated cells by DESeq2 [31]. The DE changes in our experiments represent differences
139 in relative abundance of the small pool of mRNA that is not degraded. We infer that
140 mRNAs that appear upregulated (described throughout as relative "upregulation")
141 actually decrease in abundance, but to a lesser extent than the general population, due
142 to resistance to RNase L cleavage activity or compensation by active transcription. The
143 DE values therefore characterize how the global loss of mRNA varies across the
144 transcriptome. We found hundreds of differentially expressed genes ("DE genes,"
145 $p_{adjusted}<0.05$) in 2-5A treated WT cells, revealing that the level of these mRNAs
146 significantly differs from the baseline loss that generally affects all transcripts (Figure 1B).
147 2-5A treatment did not induce many changes in differential gene expression in *RNASEL*
148 KO cells (Table S1), as expected, since 2-5A is a specific activator of RNase L. DE genes
149 that appeared to be upregulated by RNase L activation (Figure 1B), defined as log2 fold
150 changes >1) included transcripts that encode proinflammatory proteins and cytokines
151 (e.g. *CXCL2*, *CCL20*, *CXCL8*, and *IL6*), suggesting that direct RNase L activation
152 stimulates an inflammatory response. In contrast, we did not detect an interferon (IFN)
153 response, such as increased transcript levels for *IFNB1.* These findings are largely
154 consistent with previous RNA-seq data from human cells (WT vs *RNASEL* KO) that were
155 transfected with poly I:C [16,17]. These changes were consistent across replicates (Figure
156 S1B).
157 We noted that some of the genes that appear to be upregulated in 2-5A treated
158 cells encode transcription factors or activators, such as *JUN*, *FOSB*, *FOXA2*, *GDF15*, and
159 *ATF3* (Figure 1B). This is consistent with previous findings for some of these genes, such

160 as *FOXA2* and *GDF15* [14,32]. Gene Ontology (GO) analysis of molecular functions offered
161 additional support since several of the top categories of DE genes were related to
162 transcription regulation (Figure 1C). This finding suggests that the apparent increase in
163 some transcript levels in our DE analysis could be due to new transcription that is induced
164 by these factors. Since RNase L reduces global mRNA levels in the cell, it is unclear
165 whether the relative upregulation of these transcription factor genes observed in our RNA-
166 seq data is sufficient to increase production of protein. Thus, we probed selected
167 transcription factor protein levels by western blotting. Interestingly, we found that protein
168 levels for FOSB and JUN increased in 2-5A treated WT, but not *RNASEL* KO, cells
169 (Figure 1D and S1C). This finding suggests that activation of RNase L can actually raise
170 the abundance of these proteins, leading to downstream transcriptional activation.

171 Next, we assessed which pathways are triggered in 2-5A treated cells that could
172 explain the apparent transcriptional upregulation. We found that several target genes in
173 the JNK, p38, ERK, and NF-κB pathways appeared to be increased in our data,
174 suggesting that at least some of these pathways (which are known to have overlapping
175 targets) are activated. For instance, the transcription factor GDF15 controls inflammation,
176 cell repair, and growth, and is known to be upregulated by the activity of the JNK and
177 ERK kinases when prostate cancer cells are treated with 2-5A [14]. To dissect which of
178 these pathways are specifically responsible for the observed transcriptional changes in
179 our dataset, we used western blotting to assess activation through phosphorylation of
180 these pathways. We found that RNase L can activate JNK and p38 (Figure 1E and S1D),
181 but we did not detect activation of pathways related to ERK (Figure S1E, ERK
182 phosphorylation) or NF-κB (Figure S2, p65 nuclear fraction). These results suggest that
183 transcriptional changes observed in the cells here are driven, in part, by the activation of
184 JNK and p38. We also noticed that multiple *DUSP* mRNAs, such as *DUSP1* and *8*, that
185 encode negative regulators of the JNK pathway were upregulated (Figure 1B and S1B),
186 suggesting a need for modulation of JNK when RNase L is activated. Interestingly, JNK
187 activation can be apoptotic or induce autophagy. Here we observed the induction of
188 proapoptotic genes, such as *JUN*, but not genes expressed during autophagy, such as
189 *ATF5* [33].

190 It has been suggested that activation of RNase L can trigger the RSR, which can
191 lead to downstream activation of the JNK and p38 pathways [23,25]. Since it was
192 demonstrated that this can involve the ribosome collision sensor and kinase, ZAKα, we
193 tested whether ZAKα is activated in 2-5A treated cells by examining its phosphorylation
194 state by western blotting. We found that ZAKα is strongly activated due to 2-5A treatment
195 in WT but not in *RNASEL* KO cells, indicating that phosphorylation of JNK and p38 under
196 RNase L might occur through ribosome collisions during RNase L activation (Figure 1E-
197 F and S1D).
198

199 **The OAS-RNase L pathway acts together with other dsRNA sensing pathways to**
200 **achieve strong activation of innate immune signaling**

201 We next asked whether activation of RNase L modulates the effects of other
202 pathways that are typically activated during infection by other dsRNA sensors [18,19]. To
203 simultaneously activate multiple pathways and test RNase L's role, we transfected WT
204 and *RNASEL* KO A549 cells with poly I:C, a dsRNA mimic (0.25 µg/ml) and performed
205 RNA-seq (Figure 2A). Poly I:C is known to strongly activate OAS and, in turn, RNase L
206 as well as other dsRNA sensing pathways, including PKR, and RIG-I/MDA5. First, we
207 assessed the levels of RNase L activation by measuring the level of rRNA degradation
208 and comparing it to that in cells treated by the direct activator, 2-5A. We found that in all
209 replicates of poly I:C and 2-5A treated cells, the level of rRNA degradation was
210 comparable (within 2-fold), suggesting a similar level of RNase L activation (Figure S1A).
211 Next, we determined the DE genes in WT cells upon poly I:C treatment with
212 DESeq2. We found that poly I:C treatment resulted in a higher number of relatively
213 upregulated DE genes (~1200, log2 fold changes >1, $p_{adjusted}$ <0.05) as compared to 2-
214 5A treatment (~700 genes) and that additional pathways were activated, as expected
215 given the broader effects of poly I:C (Figure 2B). In particular, in both WT and *RNASEL*
216 KO cells, PKR and RIG-I/MDA5 pathways were activated, as judged by increased levels
217 of eIF2α phosphorylation (shown previously in [21] and discussed further below) and the
218 increase in ISGs (Figure 2C and Table S1), respectively. Consistent with this, we
219 observed that *PPP1R15A* (*GADD34*), a gene involved in the ISR (see below) and known
220 to be transcribed as a result of both interferon production via the IRF3/7 pathway and

221 PKR activation [34], also exhibited a relative increase compared to other transcripts (~32-
222 fold) in poly I:C treated WT cells (Table S1 and Figure 2C).
223 Notably, we also found that most genes that are differentially expressed upon 2-
224 5A treatment were also differentially expressed in poly I:C treated cells (Figure 2B, note
225 overlap between yellow- and magenta-colored circles, Pearson's R^2=0.92). This suggests
226 that these changes are largely unimpaired in cells treated with poly I:C and are not
227 masked by the effects of the other activated dsRNA pathways. We noted that many genes
228 that did not meet the criteria for significant differential expression in WT cells treated with
229 2-5A changed in ways that closely mirrored changes observed in cells treated with poly
230 I:C (Pearson's R^2=0.75 for DE genes this subset). This correlation indicates that the small
231 relative gene expression changes in 2-5A treated cells that do not meet the DE threshold
232 may indicate partial activation of pathways that get amplified when other dsRNA sensors
233 are triggered in poly I:C treated cells.
234 To more closely investigate how simultaneous activation of RNase L and other
235 pathways triggered by dsRNA affects the JNK and p38 pathways, we examined the
236 mRNA levels of target genes and phosphorylation of the proteins themselves. Based on
237 our finding above that 2-5A treatment (RNase L activation alone) activates the JNK and
238 p38 pathways (Figure 1E, Figure 2C, blue dots), we defined a subset of 54 transcripts
239 that are commonly associated with JNK and p38 and are activated in 2-5A treated
240 samples (see Methods section for more details). Since ~50% of the genes downstream
241 of JNK and p38 overlap, we analyzed these MAPK pathways together. We assessed
242 transcriptional induction of JNK/p38 downstream targets under activation of RNase L only
243 (WT + 2-5A), other dsRNA pathways only (*RNASEL* KO cells + poly I:C), or both pathways
244 (WT + poly I:C) (Figure 2D). As expected based on the selection of targets, we found that
245 these JNK/p38-related mRNAs were highly induced in WT + 2-5A treated cells. We also
246 noted some activation due to other dsRNA pathways alone (*RNASEL* KO + poly I:C).
247 Interestingly, when combined, the RNase L and other dsRNA pathways together
248 suggested the effects may be additive since the level of induction was highest in WT cells
249 treated with poly I:C (Figure 2D). We therefore asked whether these trends were
250 supported by the level of JNK and p38 phosphorylation, as measured by western blotting
251 (Figure 2E). In support of additivity between the RNase L and the other dsRNA pathways,

252 we observed the strongest phosphorylation of JNK and p38 when both RNase L and the
253 other dsRNA pathways were triggered compared with either one alone (Figure 2E and F).
254 In addition, we found that ZAKα, which we showed to be phosphorylated by 2-5A
255 treatment (Figure 1E) was also phosphorylated in poly I:C treated WT cells to a similar
256 extent, suggesting that activation of ZAKα by RNase L is not affected by the other dsRNA
257 pathways (Figure 2E). Importantly, ZAKα phosphorylation was not detectable in *RNASEL*
258 KO cells that were treated with poly I:C, suggesting its activation (presumably via
259 ribosome collisions) requires RNase L activity. This model therefore implies that JNK and
260 p38 phosphorylation in the absence of RNase L (Figure 2E) must use a MAP3K other
261 than ZAKα and that, together with ZAKα, affords the strongest induction of p38/JNK
262 targets in cells treated with poly I:C (Figure 1E).
263 Activation of ZAKα by ribosome collisions can simulataneously occur with
264 activation of the GCN2 kinase, which phosphorylates eIF2α and is also activated by
265 ribosome collisions [25,27]. Hence we wondered if RNase L could contribute to eIF2α
266 phosphorylation through ribsome collisions. We did not detect eIF2α phosphorylation
267 after 2-5A treatment, consistent with previous reports [5,21]. However, we found that eIF2α
268 phosphorylation levels were substantially decreased in poly I:C treated *RNASEL* KO cells
269 as compared to WT cells (Figure 2E and F), which is also consistent with previous reports
270 [17]. This finding shows that activation of RNase L increases eIF2α phosphorylation under
271 some conditions, perhaps by enhancing PKR activation, activating another kinase such
272 as GCN2, and/or reducing the activity of an eIF2α phosphatase.
273 Next, we assessed if activation of RNase L affects the interferon response that is
274 triggered by dsRNA binding to MDA5 and RIG-I (Figure 2C, red dots). We defined a
275 subset of ISGs (N = 45, see Methods for details) that were upregulated in WT cells treated
276 with poly I:C. We then looked at the activation of these genes across our experimental
277 conditions (Figure 2D, right panel). We found no activation of these genes with 2-5A
278 treatment, consistent with previous RNA-seq findings in A549 cells [16,17,21], but contrasting
279 with models where RNase L cleaved RNA fragments stimulate other dsRNA sensors,
280 potentially in other cell lines [18,19]. In cells treated with poly I:C, we observed some
281 decrease in activation for this limited subset of genes in *RNASEL* KO cells compared to

282 WT cells (Figure 2D). This finding suggests that RNase L may have a minor role in
283 augmenting activation of other dsRNA sensors in these cells [18,19]. We further investigated
284 these trends by western blotting (Figure 2E and F). In these experiments, we visualized
285 the phosphorylation of IRF3, one of the main transcription factors that induces ISGs in
286 response to interferon. We were unable to detect activation of IRF3 in cells treated with
287 2-5A but observed activation in cells treated with poly I:C, in agreement with our RNA-
288 seq analysis. We also observed a small decrease (~20%) in activation of IRF3 in *RNASEL*
289 KO cells treated with poly I:C, in line with our observations from RNA-seq and a previous
290 report [17]. This supports a model where RNase L may have some role in affecting the
291 response to interferon.
292 We also asked whether RNase L can contribute to the other pathways that play a
293 role in the dsRNA-induced innate immune response, such as NF-κB and ERK. Activation
294 of NF-κB (p65) was only detectable in poly I:C treated cells and the levels of activation
295 appeared to be similar in both WT and *RNASEL* KO cells, indicating that RNase L has no
296 further effects on this pathway (Figure S2). We also found that 2-5A or poly I:C treatments
297 had no effect on ERK activation in A549 cells, suggesting that the observed effects in our
298 experiments are not due to activation of ERK (Figure S2).
299 Taken together, our analysis shows that activated RNase L can act together with
300 other dsRNA pathways to promote p38 and JNK signaling, but has only minor effects on
301 the activation of IRF3 (Figure 2G).
302
303 **A generic endonuclease, RNase A, induces transcriptional changes similar to**
304 **those triggered by RNase L**
305 Next, we wanted to assess what changes directly result from the global RNA
306 cleavage that occurs after RNase L activation. RNase L is known to interact with several
307 proteins, including those that make up the cytoskeleton and the nucleopore complex [35-
308 40]. Thus, it is possible that some of the observed changes upon RNase L activation and
309 dimerization arise from functional protein-protein interactions and not RNA cleavage. To
310 further investigate how global RNA cleavage changes gene expression, we
311 electroporated a generic RNase, RNase A (bovine pancreatic ribonuclease), in *RNASEL*
312 KO A549 cells and performed RNA-seq after 4.5 hours (Figure 3A). RNase A is a small

313 endonuclease that primarily cleaves at pyrimidine bases (U and C) in ssRNAs [41,42]. As a
314 control, we electroporated similar amounts of Bovine Serum Albumin (BSA) since it is
315 similar in size, but has no RNase activity. We anticipated that RNase A would cause
316 widespread RNA decay but would lack RNase L specific interactions. During our
317 experiments, we followed RNase A activity by monitoring rRNA cleavage, similar to our
318 above experiments with RNase L. We observed that rRNAs are degraded in RNase A
319 electroporated cells, but with different RNA cleavage patterns (Figure S3A). Based on
320 RNase A's low level of specificity, we expect that most RNA species (including mRNAs)
321 would be targeted and thus fragmented by RNase A.

322 We found >1000 differentially expressed genes in RNase A electroporated cells
323 (Table S1). As noted for RNase L activation above, gene expression is reported in
324 absolute terms from the average global loss of mRNA; therefore, genes that appear to be
325 upregulated may simply be less downregulated than those in the same treatment group.
326 Interestingly, most upregulated DE genes found in 2-5A treated cells overlap with those
327 identified here for RNase A activation (~65 % of those in the RNase L dataset, Figure 3B
328 and C, Figure S3B) and the expression levels showed correlation (Pearson's R^2 = 0.39,
329 Figure 3C). This suggests that most RNase L-dependent DE changes are the direct result
330 of RNA cleavage rather than potential indirect non-enzymatic activities.

331 Next, we assessed if targets of the JNK signaling pathway were upregulated in
332 RNase A electroporated cells as they were in 2-5A treated ones. We found that the JNK
333 and p38 pathway-related mRNAs were upregulated in RNase A electroporated samples
334 (Figure 3D). JNK and p38 phosphorylation were also confirmed by western blotting
335 (Figure 3E). Strikingly, we found that ZAKα was also phosphorylated (Figure 3E). Our
336 results therefore indicate that transcriptional changes, particularly through the JNK and
337 p38 pathways, can be induced by non-specific RNA cleavage, regardless of the effector
338 endonuclease.

339

340 **RNA fragmentation by generic RNases induces altORF translation**

341 Previously, we examined the translation that takes place in RNase L activated cells
342 by using ribosome profiling to find where ribosomes translate the reduced pool of mRNAs
343 [21]. One of the most striking findings from our previous study is that the relative abundance

344 of ribosome footprints increased in non-coding regions of transcripts, including the 5' and
345 3' UTR regions, as well as out-of-frame parts of coding sequences. This phenomenon
346 likely results when ribosomes initiate translation at the first available open reading frame
347 on the 3' mRNA fragments that are generated by RNase L, a phenomenon that we termed
348 "altORF translation" [21]. The model predicts that the activity of any generic endonuclease
349 should lead to the same outcome. To test this hypothesis, we electroporated RNase A
350 into *RNASEL* KO A549 cells, as described above, and performed ribosome profiling on
351 those same samples after 4.5 hours (Figure 4A).

352 The major hallmarks of altORF translation that we previously observed in RNase
353 L activated cells were recapitulated in the cells where RNase A was electroporated
354 (Figure 4B-D). The most striking signature of altORF translation is a relative increase in
355 ribosome footprints in the 3'UTR. This region of the mRNA is rarely translated under
356 normal conditions, but we found ribosomes in this region when RNase L was active [21].
357 Cells where RNase A was active exhibited similar ribosome profiling patterns in the
358 3'UTRs, consistent with the altORF translation model (Figure 4B, *ACTG1* as an example
359 gene model). We also investigated whether this signature was present in RNase-A
360 treated samples globally. To assess characteristics of altORF translation in a global
361 manner, we computed the ratios of ribosome profiling footprint levels in 3' UTR regions
362 and the main ORFs of mRNAs (3'UTR:ORF ratios) as we did before for active RNase L.
363 We found that in all RNase treated samples, 3'UTR:ORF ratios increased compared to
364 respective controls (Figure 4C) [21]. Increased 5'UTR:ORF ratios were also observed in
365 RNase L activated cells [21] and we found similar patterns when computing 5'UTR:ORF
366 ratios for RNase A treated cells, pointing to higher relative levels of altORF translation in
367 these samples (Figure S4A). Increased reads in the 5' and 3'UTRs were also observed
368 in metagene averages at the start and stop codon of main ORFs for RNase A
369 electroporated samples as compared to the control (Figure 4D and S4B), further
370 confirming increased relative ribosome occupancy and potential altORF translation in the
371 UTR regions.

372 The data from cells that were electroporated with RNase A suggest the
373 phenomenon of altORF translation takes place whenever any generic endonuclease, not
374 only RNase L, is active in the cytoplasm. However, electroporation of RNase A is artificial,

375 and we wondered whether another naturally activated endonuclease would trigger the
376 translation of altORFs. The endonuclease IRE1 is homologous to RNase L and plays a
377 pivotal role in the Unfolded Protein Response (UPR) since it is activated by protein
378 misfolding in the ER [43]. IRE1 is required for cytoplasmic splicing of the *XBP1* mRNA
379 through recognition of specific sequences and structural elements. However, IRE1 can
380 also cleave more generically at UGC sequence motifs. This broader activity is referred to
381 as Regulated IRE1 Dependent Decay (RIDD) and could potentially lead to altORF
382 translation [29,44]. To test this hypothesis, we analyzed a publicly available ribosome
383 profiling dataset where human cells were treated with thapsigargin, a potent inducer of
384 the UPR and IRE1 [45] (GEO ID: GSE103719). We found that thapsigargin-treated cells
385 also exhibited characteristics of altORF translation, including increased 3'UTR:ORF ratios
386 (Figure 4E). These results show that RNase L is not the only naturally activated
387 endonuclease that can lead to the translation of altORFs.
388
389 **RNA fragmentation can modulate translational efficiency**
390 The major effect on gene expression of active RNase L is that the majority of
391 mRNAs are lost, resulting in reduced protein synthesis for most genes. However,
392 transcriptional upregulation counteracts this and, in some cases, overrides (Figure 1D)
393 this effect. In addition, it is conceivable that gene expression from the remaining mRNAs
394 could be tuned at the translational level and thus further refine the amount of protein
395 synthesized from the remaining transcriptome. As an example of this, an increase in the
396 translation of some host mRNAs was reported during vaccinia virus infection, which is a
397 potent activator of RNase L [46]. In this way, mRNA degradation could have a role in
398 regulating translation.
399 To investigate whether RNase L activity alters which mRNAs are translated, we
400 took advantage of our ribosome profiling data (reported previously [21]) and with its
401 matched RNA-seq data (reported here) assessed translational efficiency (TE) of coding
402 sequences. The TE metric is defined as the ribosome footprint level in a coding region,
403 normalized to the corresponding RNA-seq level, and serves as a proxy for the relative
404 loading of a transcript by ribosomes. We therefore plotted the change in ribosome
405 footprint levels against the corresponding change in RNA-seq level (Figure 5A) for genes

406 where either of these values were found to change significantly by DESeq2 (see
407 Methods). Those genes with large changes in TE will appear furthest from the diagonal
408 (slope >1 indicates TE increase; <1 TE decrease). We noted several cases where dots
409 were shifted from the diagonal, suggesting functionally important regulation of translation.
410 Some of the largest changes we observed affected a group of transcripts that were
411 expressed at higher relative levels when RNase L was active at the mRNA level (via 2-
412 5A or poly I:C in WT, but not in *RNASEL* KO, cells) but were counterbalanced by
413 downregulation of expression at the translational level (lower TE, Figure 5A, dots to the
414 right of the origin and below the dotted diagonal). This category includes the extracellular
415 matrix proteins *MUC5AC* and *MUC5B* (Figure 5A). We directly computed the TE for these
416 genes for each replicate and found the effect of reduced TE to be consistent (Figure 5B).
417 We also noticed an enrichment for genes encoding proteins involved in transcription or
418 related to transcription in this category (e.g. *KLF6*, *ZNF296*), suggesting that RNase L
419 tunes the production of proteins involved in transcription at the translational level.
420 In another class of genes, we observed that relative mRNA levels were increased
421 upon RNase L activation (via 2-5A or poly I:C in WT, but not in *RNASEL* KO, cells) and
422 that the level of ribosome footprints also increased to a larger extent and would therefore
423 be expected to augment gene expression (Figure 5A, dots to the right of the origin and
424 above the dotted diagonal). This category included *CXCL1-3* and *8*, genes that encode
425 chemokines and cytokines. We also directly computed the TE for these genes for each
426 replicate and found the effects to be consistent (Figure 5B). Interestingly, we found that
427 mRNAs encoded by the mitochondrial genome also fell into this category (Figure 5A,
428 orange dots). This observation is consistent with a study of TEs during vaccinia infection
429 where higher levels of translation of mitochondrially-encoded transcripts in conjuction of
430 higher oxidative phosphorylation activity was reported. This was proposed to enhance
431 viral replication due to its high energy demand [46]. Our data therefore suggest that this
432 phenomenon is driven by RNase L.
433 Intriguingly, we also observed a trend among mRNAs that are induced by dsRNA
434 pathways apart from RNase L, including *IFIT1-3* and *IFNB1* (induced by interferon) and
435 the gene *GADD34* (induced by interferon and the ISR as noted above). These genes
436 exhibited ~2 fold higher TEs in poly I:C treated *RNASEL* KO cells as compared to WT

437 cells (Figure 5A, dots shift above diagonal in right vs middle panel), suggesting that
438 RNase L may play some role in reducing their expression at the translational level as a
439 way to tune their transcriptional induction.
440
441 **RNase L activation modulates the Integrated Stress Response**
442 Given the role of *GADD34* in the ISR, we further examined the ribosome profiling
443 data for clues as to how its translation is regulated by RNase L. The ISR is activated when
444 PKR binds dsRNA and phosphorylates the translation initiation factor eIF2α, ultimately
445 resulting in a loss of its ability to promote translation initiation [47]. The downstream effects
446 of eIF2α phosphorylation are collectively known as the Integrated Stress Response (ISR)
447 [11,12]. Phosphorylation of eIF2α generally limits the loading of ribosomes on mRNAs in the
448 cell, reducing their TE. However, there is a small class of mRNAs, including *ATF4*,
449 *GADD34* (*PPP1R15A*), and *CHOP* (*DDIT3*), that undergo the opposite response and are
450 translationally activated [11]. ATF4 and CHOP are transcription factors that induce
451 expression of stress-responsive genes, while GADD34 is a phosphatase of eIF2α and
452 thus serves as a counterbalance to ISR activation [48,49]. We found that relative transcript
453 levels increased in poly I:C treated WT and *RNASEL* KO cells as compared to respective
454 controls for *GADD34* (as noted above, 5-32-fold) and *CHOP* (5-9-fold) (Table S1). This is
455 consistent with work showing both genes are transcriptionally induced by ATF4 [50,51].
456 *GADD34* is likely further induced by the interferon-induction IRF3 pathway [34]. The
457 *GADD34* mRNA was identified as a strong target of RNase L driven degradation [17] and
458 thus absolute levels of *GADD34* are likely lower in WT cells as compared to *RNASEL* KO
459 cells. The transcripts for *ATF4*, *CHOP*, and *GADD34* contain one or more open reading
460 frames in their 5'UTR (uORFs) with unique features that allow them to suppress
461 translation of the main ORF in non-stressed cells, but activate it when eIF2α becomes
462 phosphorylated [11,52]. As noted above, the TE for *GADD34* was observed to increase in
463 poly(I:C) treated cells (WT or *RNASEL* KO) (Figure 6A), though 2-fold less in WT than
464 RNASE L KO cells.
465 Several explanations could account for our observation that the change in
466 *GADD34* TE was less in WT vs *RNASEL* KO cells (Figure 6A). One possibility is that
467 RNase L could directly affect TE by altering the shift in translation from the uORFs to the

468 main ORF. To determine whether RNase L had an effect on uORF-based regulation, we
469 quantified the ratio of ribosome footprints in the 5'UTR and compared it to footprints that
470 mapped to the main ORF (Figure 6B-C, see Methods). We noted a substantial decrease
471 in uORF translation relative to main ORF translation in poly I:C treated WT or *RNASEL*
472 KO cells due to eIF2α phosphorylation, as expected [52]. However, this decrease was less
473 in the case of the WT cells compared to *RNASEL* KO cells (Figure 6B-C), suggesting that
474 RNase L activation may have some role in affecting this shift. Similar RNase L dependent
475 shifts in 5'UTR vs main ORF ribosome footprints for *ATF4* and *CHOP* suggest this
476 regulation may also extend to those genes (Figure S5A-B). It has been shown that the
477 *GADD34* mRNA is heavily targeted by RNase L, making the mRNA and protein product
478 in poly I:C treated *RNASEL* KO cells much more detectable than in WT cells [17]. Consistent
479 with this, we also found that GADD34 protein levels increased in poly I:C-treated *RNASEL*
480 KO cells (Figure 6D). Thus, this mechanism where RNase L suppresses main ORF
481 translation augments the underlying trend in expression that is driven by mRNA decay.
482 Taken together, these results show a role of RNase L in inhibiting the translation
483 of *GADD34*, thus modulating the ISR during the innate immune response, and suggests
484 the RNase L may have a broader role in regulating translational control.
485
486 **Translation of IFIT mRNAs is inhibited by activation of RNase L**
487 Since we observed that poly I:C induced higher translation efficiency in *RNASEL*
488 KO vs WT cells for the genes *IFIT1*, *2*, and *3* (Figure 5A, right panel), we asked whether
489 this trend could be explained by uORF-mediated translational control as in the case of
490 the ISR-related mRNAs. IFIT proteins are one of the key antiviral proteins that are
491 stimulated by interferon and inhibit viral translation [53]. Since these genes have low
492 expression under conditions without poly I:C stimulation, we focused on data from cells
493 treated with poly I:C.
494 To determine whether uORFs were translated on these mRNAs, we examined
495 ribosome densities in their 5'UTR in ribosome profiling data. We found that 5'UTRs of
496 *IFIT1*, *2* and *3* contained ribosome peaks at start codons of potential uORFs (Figure 7A
497 and Figure S6A, green lines). The uORFs used near-cognate start codons (CUG or GUG
498 instead of AUG, Figure 7A and Figure S6A). These data suggest a model for translational

499 control where the uORFs inhibit main ORF translation and it is conceivable that this
500 inhibition could be regulated by eIF2α phosphorylation. As in the case of *GADD34* and
501 other genes, this apparent uORF inhibition may be regulated by RNase L since there was
502 lower 5'UTR translation relative to main ORF translation in poly I:C treated *RNASEL* KO
503 vs WT cells that was correlated with higher TE (Figure 7B and C). These data further
504 imply that expression of these genes may be controlled by inhibitory uORFs and that this
505 mechanism may depend on RNase L (Figure 7D). We also found that IFIT1 and IFIT2
506 protein levels increased in poly I:C-treated *RNASEL* KO cells compared to WT cells
507 (Figure S6B). This change is consistent with the reduction in translation efficiency or
508 mRNA loss in WT cells.
509
510 **Discussion**
511 In this study, we examined how direct RNase L activation by 2-5A, and attendant
512 global RNA degradation in the cell, affects gene expression. Our work shows that the
513 global loss in mRNA is compensated by increases in transcription, particularly via
514 activation of ZAKα, and tuned by changes in translation.
515 We showed that one way mRNA cleavage leads to new transcription is via
516 activation of the RSR. RNase L activation alone (via 2-5A) turns on the p38 and JNK
517 MAPK pathways, independently of other dsRNA sensors that are activated by poly I:C
518 (Figure 1). While JNK activation was previously documented in several cell lines,
519 simultaneous p38 activation was not observed when RNase L alone was activated [14,23].
520 Since poly I:C treatment strongly induces p38, it is possible that weak activation of p38
521 was masked in previous studies, or the extent of activation could be cell line dependent.
522 The activation of JNK is known to be associated with the RSR [54,55] and it was initially
523 suggested to be involved in innate immunity due to damage to rRNA by RNase L [22,23].
524 However, more recent studies showed that even with their rRNA damaged by RNase L,
525 ribosomes can still translate [16] and may therefore not be neccesarily responsible for RSR
526 activation. Recently, it was found that the RSR can be activated by the ribosome collision
527 sensor and MAP3K, ZAKα [25,27]. We established that ZAKα can also be triggered directly
528 by RNase L activity, but not by the other dsRNA pathways. Moreover, it is likely that other
529 mechanisms, beyond the RSR, exist to activate transcription in response to global RNA

530 degradation. For instance, global RNA loss in the cytoplasm was proposed to free up
531 RNA binding proteins that, in turn, modulate transcription due to their relocation to the
532 nucleus [56].

533 Our observation raises the question of why ribosome collisions might be occurring
534 in these cells. Ribosome collisions are known to form when a ribosome stalls during
535 elongation and upstream ribosomes bump into it [57]. One possibility is that mRNAs
536 undergoing active translation are cleaved by RNase L, resulting in the ribosomes stalling
537 whenever they reach a 3' end of a 5' cleavage fragment. Prior work using ribosome
538 profiling demonstrated this kind of 3'-end stalling and formation of ribosome collisions
539 when the homologous nuclease, Ire1, cleaves mRNAs during the unfolded protein
540 response in fission yeast [29]. Consistent with the idea of an increase in ribosome collisions
541 during viral infection, it was shown that vaccinia virus infection leads to an increase in
542 ubiquitination of the ribosomal protein uS10 by the ubiquitin ligase ZNF598, which is
543 known to be directly activated by ribosome collisions [58]. Alternatively, ribosome collisions
544 could form for other reasons, including the widespread translation of alternative (non-
545 canonical) ORFs that we previously reported [21], since such ORFs may be less
546 evolutionarily tuned to minimize slow translation [59]. We also note that ZAKα has been
547 reported to be somewhat activated by individual stalled ribosomes, implying ribosome
548 collisions are not strictly required for the effects observed here [60]. It is also possible that
549 ZAKα could be activated in other ways that involve the cleaved RNA fragments through
550 a yet unknown mechanism. The effect of RNase L-induced activation of the RSR was
551 previously shown to be JNK-mediated programmed cell death in response to viral
552 infections [22]. Interestingly, both ZAKα and RNase L activation were shown to trigger the
553 inflammasome independently [20,28]. Considering our data, it is plausible that RNase L also
554 triggers inflammasome activation through ZAKα, and contributes to cell death.

555 Previous RNA-seq studies hinted that RNase L activation may act together with
556 the other dsRNA pathways to amplify the innate immune response [17]. Our findings here
557 confirm this synergy by showing that activation of JNK and p38 occur by both RNase L
558 dependent and independent routes. Since impairment of RNase L activation can have
559 serious health consequences linked to a reduced ability to fight viral infections [61,62], it is
560 possible that the loss of this two-pronged activation weakens other branches of the

561 immune response that are independently triggered by dsRNA. In addition, our observation
562 that ERK is not activated and p38 is activated by 2-5A has not been consistently observed
563 in previous studies [14,23], further suggesting that the activation of kinases by RNase activity
564 is regulated by other factors, possibly in a cell-line dependent way.

565 Interestingly, our data also suggest that RNase L may lead to further regulation of
566 eIF2α kinase activity. Our analysis of eIF2α phosphorylation levels in cells treated with
567 poly I:C shows that phosphorylation is higher when RNase L is active. This is consistent
568 with previous reports showing that besides PKR, another kinase can phosphorylate eIF2α
569 during poly I:C treatment and it is dependent on RNase L activity [17]. A possible
570 explanation is that RNase L activates the eIF2α kinase GCN2, which is sensitive to
571 ribosome collisions [25,63-65] and enhanced by ZAKα activation [25]. Intriguingly, our analysis
572 and previous studies [5,21] of eIF2α phosphorylation levels suggest direct RNase L
573 activation via 2-5A does not activate any kinase of eIF2α. Therefore, enhanced
574 phosphorylation of eIF2α when RNase L is active likely relies on additional factors that
575 are activated by poly I:C but are absent when only RNase L is active.

576 Beyond control of new transcription, we also examined roles for RNase L in
577 changing which transcripts are translated. We noted several prominent cases (Figure 5)
578 where mRNA TEs were changed when RNase L was activated by 2-5A. The mechanism
579 underlying these translational changes remains unclear, however, several possible
580 explanations exist. Certain transcripts, such as *IFNB1*, are retained in the nucleus via
581 direct interactions with nucleopores when RNase L is activated [35] or a viral nuclease is
582 activated [66]. This mechanism would explain the apparent decrease in translational
583 efficiency of this gene (decreased TE in poly I:C treated WT as compared to *RNASEL*
584 KO, Figure 5) and possibly other transcripts due to selective retention in the nucleus. In
585 addition, TE changes could arise because the availability of ribosomal subunits and the
586 corresponding translation machinery, such as initiation factors, likely increase because
587 the overall level of mRNA is greatly reduced upon RNase L activation [16,67]. Such a
588 dramatic change in this "ribosome homeostasis" (as defined, [68,69]), or balance between
589 mRNA and the translational machinery, has been shown to result in changes in which
590 transcripts are favored for translation [70,71]. Such a result is thought to occur because
591 mRNAs that are generally less efficient at recruiting ribosomes can be more heavily

592 translated due to an abundance of ribosomal subunits promoting translation via mass
593 action.

594 We also focused on changes in translation efficiency related to the ISR since it is
595 a well-established regulatory pathway known to rely on control of translation via
596 phosphorylation of eIF2α by the dsRNA sensor PKR [11,52]. One consequence of eIF2α
597 phosphorylation is the translational activation of a set of genes, such as *GADD34*, due to
598 a shift in translation initiation from uORFs to the main ORF [11]. Intriguingly, we found that
599 activation of RNase L overrides this effect of eIF2α phosphorylation and limits the
600 translational activation of *GADD34*. This translational suppression would serve to further
601 enhance the inhibition of this gene due to its known susceptibility to RNase L mediated
602 degradation (Figure 6) [17]. One possible explanation for the inhibitory effect of RNase L on
603 the translation of this gene is that the availability of eIF2α may increase when RNase L is
604 active due to the general reduction in demand for translation, as noted above. As a result,
605 the impact of phosphorylation of eIF2α on translation initiation may be lessened, thus
606 preventing the shift from uORF to main ORF translation on these transcripts. Alternatively,
607 since RNase L cleaves rRNAs, it is plausible that this damage could alter the choice of
608 start codon (uORF vs main ORF) by scanning 40S subunits. Another possibility is that we
609 previously showed [21] that RNase L activation leads to an increase in the proportion of
610 ribosome footprints in 5'UTRs globally and this holds true for *GADD34* (Figure 6B-C).
611 This effect may arise from direct initiation on mRNA cleavage fragments generated when
612 RNase L cleaves in the 5'UTR. This change in initiation could therefore lead to the
613 reduced translational activation of *GADD34*. Interestingly, we also found that eIF2α
614 phosphorylation levels were decreased in poly I:C treated *RNASEL* KO cells compared
615 to WT. Since GADD34 directly dephosphorylates eIF2α, we postulate that increased
616 amounts of GADD34 protein in poly I:C treated *RNASEL* KO cells could contribute to the
617 decrease of eIF2α phosphorylation.

618 Additionally, we found that RNase L-dependent changes in translation efficiency
619 of *IFIT1*, *IFIT2*, and *IFIT3* (as well as other interferon-related transcripts) is correlated with
620 an apparent shift in uORF to main ORF translation. One potential explanation for this
621 effect is that these *IFIT* genes, much like *GADD34*, could be activated by the ISR. In this
622 scenario, RNase L would similarly serve to limit their activation. While the expression of

623 these genes is likely already downregulated at the mRNA level by RNase L mediated
624 degradation, this mechanism offers additional control and suppression. Such dampening
625 could be important for limiting autoimmune conditions. For example, impairments in the
626 OAS-RNase L pathway is one of the contributing factors for MIS-C (Multisystem
627 Inflammatory Syndrome in Children) [72]. In the case of MIS-C, the disease appears to
628 manifest due to the lack of RNase L's control of inflammation. Thus, active RNase L may
629 serve a dual role in innate immunity, activating key pathways while counterbalancing
630 others.

631 Finally, we found that the generic endonuclease RNase A evokes a transcriptional
632 response, including that mediated by ZAKα, that is very similar to that of RNase L (Figure
633 3). In addition, RNase A, or the ISR-mediated endonuclease IRE1, can also trigger the
634 translation of altORFs, much like RNase L (Figure 4). This evidence suggests other
635 endonucleases, such as the viral endonuclease Nsp1 or the apoptotic host endonuclease
636 EndoU [66,73,74], could potentially cause similar outcomes to RNase L. It is intriguing that
637 virally-encoded endonucleases may bring about outcomes that are similar to host
638 endonucleases and suggests the effects of generic endonuclease activation can be tuned
639 to benefit either the virus or the host. For example, in the case of Nsp1, nuclear mRNA
640 retention and cytoplasmic mRNA degradation were shown to be important for limiting the
641 interferon response and promoting viral replication [35,66]. On the other hand, more limited
642 dampening of these pathways, particularly for *IFNB1* [17] and *IFIT* genes shown here
643 (Figure 7), could be important for preventing autoimmune conditions or cytokine storms,
644 such as noted above. Further studies are needed to elucidate these possibilities.

645 Overall, our data offer a model where activation of RNase L induces ribosome
646 stalling and likely collisions, leading eventually to cell death via key transcriptional
647 pathways (Figure 1) related to the kinase ZAKα. This suggests that ZAKα could be a
648 potential target for therapeutics aimed at modulating RNase L's effects. This is especially
649 relevant since RNases are already being used or tested for cancer therapy, such as
650 RNase A [75,76]. We speculate that a component of the mechansim behind these RNase
651 therapies could result from ZAKα activation via ribosome collisions that occur as a result
652 of RNase activity in the cytoplasm. Thus, modulating the levels of ZAKα activation could
653 be the key for safety and efficacy of these treatments. In addition, RNase L may have

654 other roles in affecting the ISR via translation of ISR target genes. The effects of RNase
655 L on transcription and translation may be important for reinforcing or dampening effects
656 evoked by other dsRNA sensors, pointing to linkages between pathways in the innate
657 immune response. Further study is needed to dissect these connections that bring
658 together the entire spectrum of mRNA activities, including synthesis, translation, and
659 degradation.
660

Funding

This research was supported by the Intramural Research Program of the NIH, The National Institute of Diabetes and Digestive and Kidney Diseases (NIDDK) (DK075132 to N.R.G.) and the Postdoctoral Research Associate Training Program (PRAT) at the National Institute of General Medical Sciences (NIGMS) (FI2GM128743 to A.K.).

Acknowledgements

We are thankful for the insightful discussions with Drs. Bret Hassel, Alan Hinnebusch, Jon Lorsch, Stacy Horner and Tom Dever. A549 cells were a kind gift from Dr. Bernie Moss. We also thank Dr. Behdad Afzali and Dr. Daniel Chauss for their assistance with electroporation experiments and the assistance of the genomic cores at the National Institute of Diabetes and Digestive and Kidney Diseases (NIDDK) and the National Heart, Lung, and Blood Institute (NHLBI). A.K. is grateful to have been chosen for a MOSAIC K99/R00 award (K99 GM143484) and for associated mentoring support from the American Society of Cell Biology partnership activities.

Data availability

All raw sequencing (fastq) and processed alignment (wig) files are available at NCBI GEO in record GSE244176 (ribosome profiling) and GSE244125 (RNA-seq). It can be accessed with the following token for reviewer access: gdcbakkitjgrzkh (GSE244176) and anypgeyefjoxzkj (GSE244125). Custom code used for ribosome profiling in this study is available on Github: https://github.com/guydoshlab. Gene expression analysis workflow is available on https://github.com/TriLab-bioinf/TK_65_RNAseL_manuscript.

Author contributions

A.K. designed and performed experiments, analyzed the data and wrote the paper. H.A.L. performed RNA-sequencing data analysis, contributed to DESeq analysis, and edited the manuscript. A.V.D. performed western blotting experiments. N.R.G. designed experiments, developed software, and wrote the paper.

692 **Materials and Methods**

693

694 **Cell culture.** WT and *RNASE* L KO A549 lung carcinoma cells were cultured in RPMI
695 (Gibco Cat # 60870127) complemented with 10% Fetal Bovine Serum (Gibco FBS). A549
696 cells were tested and negative for Mycoplasma contamination throughout the study.
697 Mycoplasma testing was performed using eMyco Valid Mycoplasma PCR detection kit
698 (BioLink) or ATCC Universal Mycoplasma Detection Kit. Cells were incubated at 37°C in
699 the presence of 5% CO_2. Cell lines used in this study were a kind gift of Dr. Bernie Moss
700 (NIH) and generated as described in [77].

701

702 **rRNA cleavage assay.** Total RNA was extracted from ~$3x10^5$ cells using Direct-zol mini
703 kit (Zymo) or Trizol reagent (Invitrogen) according to the manufacturer's protocol. The
704 amount of total RNA was computed by absorbance at 260 nm measured by NanoDrop
705 (Thermo Fischer Scientific) and then diluted to 50-500 ng/µl. Then RNA samples were
706 run on a Bioanalyzer 2100 (Agilent) using the RNA 6000 Nano kit (Agilent) or TapeStation
707 with the Agilent RNA ScreenTape assay. Minute run-to-run shifts in band sizes are due
708 to inherent limitations of the instrument.

709

710 **Sample preparation for RNA-seq and ribosome profiling.** Cells used in experiments
711 were grown until they reached near confluency (70-90% confluent) in a T75 flask. Then
712 cells were transfected with the pre-incubated mixture of 1 µM 2-5A or 0.25 µg/ml poly I:C
713 (Invitrogen, low molecular weight) and Lipofectamine 3000 (7.5 µl/6-well) in Opti-Mem
714 serum free media as recommended by the manufacturer for 4.5 hours. Control cells
715 (definied as untreated or -2-5A) were transfected with lipofectamine only. 2-5A was
716 synthesized as described before [21]. For electroporation of RNase A or BSA, confluent
717 T75s (~6-$8x10^6$ cells) were trypsinized and resuspended in MaxCyte electroporation
718 buffer and electroporated in 3XOC25 cuvettes (MaxCyte) in the presence of 160 ng/ml
719 RNase A or BSA with standard settings for A549 in the MaxCyte ATX electroporator. Cells
720 were plated on T75 flasks and collected after 4.5 hours incubation. Then cell lysates were
721 prepared and collected as for ribosome profiling [21]. The same samples were split for RNA-
722 seq and ribosome profiling.

723

724 **Ribosome profiling.** Ribosome profiling of RNase A and BSA electroporated cells was
725 carried out as previously reported [21], except that rRNA depletion was carried out by
726 siTools riboPool rRNA depletion kit designed for human ribosome profiling. The ribosome
727 profiling data was processed and signatures of altORF translation were assessed as
728 before [21]. Sequencing was performed on HiSeq 3000 (single end 50) at the NHLBI or
729 NIDDK DNA Sequencing and Genomics Core. These ribosome profiling data and
730 previously published data were used for analysis of translation efficiency (see below).
731

732 **Total RNA-seq.** Total RNA was extracted from 100 µl of lysates prepared for ribosome
733 profiling using Direct-zol mini kit (Zymo) or Trizol reagent (Invitrogen) according to the
734 manufacturer's protocol. The amount of total RNA was computed by absorbance at 260
735 nm measured by NanoDrop (Thermo Fischer Scientific) and then diluted to 50-500 ng/µl.
736 Then RNA samples were run on Bioanalyzer 2100 (Agilent) using the RNA 6000 Nano kit
737 (Agilent). Samples for sequencing were subject to rRNA depletion and library preparation
738 by Illumina Truseq kit. Sequencing was performed on HiSeq 3000 or Novaseq 6000
739 (paired end 50 or 75 cycle) at the NHLBI DNA Sequencing and Genomics Core.
740

741 **Computational analysis.**

742 *Processing and alignment of RNA-seq reads.*

743 After removing residual adapters from sequencing reads with the bbduk.sh tool from
744 bbtools (v37.62), sequencing data were mapped to a database of highly abundant rRNA
745 and tRNA sequences with bowtie2 (v 2.4.5) [78]. Unmapped reads were then mapped to
746 the human reference genome (GRCh38) with STAR (v2.7.10a) using default parameters
747 except for alignSJDBoverhangMin=1, outFilterMismatchNmax=2,
748 alignEndsType=EndToEnd, and leaving multimaper reads mapping to less than 11 loci
749 [79]. Duplicated reads were removed with picard MarkDuplicates (v2.26.10) [80] and
750 quantification of fragments per gene was carried out with the featureCounts tool from
751 Subread software (v2.0.1) [81] using Ensembl gene annotations (Ensembl version hg38)
752 by counting read-pairs falling within coding regions (CDS) as fragments and adding

753 fractional counts for multimapper reads. BigWig files were generated with bamCoverage
754 tool from DeepTools (v3.5.1) [82].
755
756 *Analysis of RNA-seq data.*
757 Processed bulk RNaseq data was analyzed in R using the following workflow:
758 https://github.com/TriLab-bioinf/TK_65_RNAseL_manuscript. Differential gene
759 expression analysis was performed with the R package DESeq2 (v1.34.0) [31]. GO
760 enrichment analysis were carried out with the gseGO function from the R package
761 ClusterProfiler (v4.2.2) [83].
762 To identify genes associated with JNK/p38 and interferon in Figures 2C and 3C, we
763 utilized gene collections from Harmonizome 3.0 [84] that were based on Gene References
764 Into Function (GeneRIFs, JNK, p38 datasets, Table S3). Within these datasets, we used
765 a subgroup of genes that were upregulated with 2-5A treatment (JNK/p38 plots, *N*=54,
766 Table S3) to create violin plots in Figure 2D and Figure 3D. For interferon-related genes
767 in Figure 2, we used the hallmark datataset from the Molecular Signature Database [85]
768 ("interfron-gamma-response," Table S3) for a subgroup of genes that were upregulated
769 in poly I:C treated WT cells (interferon-related plots, *N*=45, Table S3). We performed
770 paired t-test to determine significant differences between the groups within each plot (see
771 legends for more details). To perform correlation analysis between datasets from cells
772 treated with 2-5A and poly I:C, we performed a sequential filtering process to compare
773 different subsets of genes according to differential expression status (see R workflow).
774
775 *Processing of ribosome profiling footprint data.*
776 Ribosome profiling data was processed as described before to remove linkers and
777 duplicates [21]. After processing, reads were 5' aligned with STAR (v2.8.2a) to the human
778 genome (hg38, UCSC). Multimapping was allowed up to 200 times (--
779 outFilterMultimapNmax option) and the maximum mismatch/read was set to 1 (--
780 outFilterMismatchNmax option). For both the RNA-seq and ribosome profiling data CDS
781 read counts were generated by featureCounts tool from Subread software (v2.0.1)
782 including multimappers as fractional counts and reads on exon-exon junctions (-M --
783 fraction and -J options, respectively).

784

785 *Analysis of translational efficiencies.*

786 We used our DESeq2 pipeline as described above for RNA-seq to obtain differential
787 expression values (log2 fold changes) for the ribosome profiling experiments. These
788 changes (RNA-seq and ribosome profiling log2 fold change values) were plotted against
789 each other in Figure 5A to visualize where translation efficiency (TE) was changing. We
790 used a filter for log2 fold changes >4 and p adjusted value <0.01 as the definition for
791 points we considered for TE changes for all datasets. We further filtered these sets for
792 normalized mean counts across the samples >50 to eliminate low expressing genes. Of
793 this reduced dataset, we excepted TE changes >2 (defined by dotted lines on Figure 5A)
794 for further consideration.The output of the DESeq2 analysis for the RNA-seq and
795 ribosome profiling are provided as Supplemental Table 1 and 2.

796 For further analysis of individual genes, we computed the TE directly by dividing reads
797 per million (rpm) values for ribosome profiling and RNA-seq data that mapped to the
798 coding sequence. This allowed us to directly compare replicates within a treatment group.

799

800 *Analysis of translation for altORF analysis and individual genes.*

801 For more detailed analysis of ribosome profiling data, we implemented a reduced-
802 transcriptome alignment and python analysis pipeline as described elsewhere [21,86]. We
803 used the Ref-Seq Select+MANE (ncbiRefSeqSelect), as downloaded from UCSC on 14
804 April 2020, for this alignment after removal of duplicates on alt chromosomes. Using our
805 python tools (writegene2) to output reads for individual gene tracks, we then computed
806 the ratio of rpm values that mapped to the UTR to those that mapped to the main ORF
807 (Figure 6, 7 and S5), based on the defined annotations. We also used these tools to
808 create metagene plots (Figure 4 and S4) using the (metagene function). When uORFs
809 overlapped the main ORF for *ATF4*, the overlap region was assigned to the UTR for the
810 calculation of UTR to ORF ratio. In general, we assume a shift of 12 nt between the 5'
811 end of a read and the P site of the ribosome. Data are displayed in individual tracks to
812 correspond with ribosome P sites.

813

814 **Western blotting.** Protein levels were assessed by SDS-PAGE electrophoresis and
815 immunoblotting during 2-5A and poly I:C treatment. For western blotting cells were grown
816 on a 6-well plate up to ~70% confluency then transfected with 2-5A or poly I:C as
817 described above. Cells were trypsinized after 4.5 hours (Gibco TrypleExpress) and
818 collected by centrifugation at 200 g for 5 minutes. The cell pellet then was resuspended
819 in 90 µl of 10 mM Tris-HCL pH=8.0, 150 mM NaCl and 1 % triton-X and incubated on ice
820 for 5 minutes. Samples were then centrifuged for 1500 rpm, 4 minutes at 4°C. The
821 supernatant was then mixed with equal amount of 2X SDS-PAGE buffer (Quality
822 Biological) and samples were sonicated with a Brenson sonicator for 10-15 seconds until
823 the sample was no longer viscous. 5-10 µl of sample was run on a 4-20% gradient Mini-
824 PROTEAN Tris-HCl gel (BioRad) or 7% PhosTag (Wako) gel prepared according to
825 manufacturer's instruction and as described before [25]. Proteins were transferred to a 0.2
826 µm PVDF membrane using the Trans-Blot Turbo System (BioRad, 1.3 A, 7 minutes for
827 4-20% gradient Mini-PROTEAN Tris-HCl gel or 1.3 A for 14 minutes for PhosTag gel).
828 Membranes were blocked in EveryBlot Blocking Buffer (BioRad) for 10 minutes at room
829 temperature. This was followed by incubation with primary antibodies overnight in TBST
830 (Tris-buffered saline plus 0.1% tween) and 1% milk. The following antibodies were used:
831 anti-p38 MAPK (Cell signaling Technologies #9212, 1:2000 dilution), anti-P-p38 MAPK
832 (Cell signaling Technologies, 1:2000 dilution, #9211), anti-IRF3 (Cell signaling
833 Technologies #11904), anti-P-IRF3 Ser396 (Cell signaling Technologies #4947), anti-
834 ZAK (Bethyl A301-993A), anti-P-JNK (Thr183/Tyr185) (Cell signaling Technologies
835 #4668), anti-JNK (Cell signaling Technologies #9252), anti-p65 (Cell signaling
836 Technologies #8242), anti-ERK1/2 (Cell signaling Technologies #4695), anti P-ERK1/2
837 (Cell signaling Technologies #4370), anti-IFIT1 (abcam #236256), anti-GADD34 (abcam
838 #236256), anti-eIF2α (Bethyl, #A300-721A), anti-P-eIF2α (abcam #32157). After washing
839 3 times for 5 minutes in TBST, secondary antibodies were incubated with the PVDF
840 membrane for 1 hour at room temperature (Goat anti-rabbit antibody, BioRad, 1:3000).
841 Then, after additional washes (3 times, 5 minutes each) in TBST, the PVDF membrane
842 were incubated with Clarity Western ECL substrate (BioRad) for 5 minutes and proteins
843 were visualized by Amersham Imager 600. Western blots were repeated for 2-4 times

using biological replicates and blots were quantified using Fiji [87]. Replicate images will be provided on Mendeley Data.

Figure Legends:

Figure 1. *RNase L activation leads to transcriptional changes through ZAK, JNK and p38.* **A** Schematics of RNA-seq experiments. A549 cells were transfected with 2-5A and RNA-seq was performed as described in Materials and Methods. **B** Volcano plot showing upregulation of example proinflammatory cytokines and transcription factors during 2-5A treatment. Differentially expressed genes define as $p_{adjusted}$ value <0.05, log_2fold change >1. **C** Gene Ontology analysis of molecular functions shows that upregulated genes are enriched in genes related to transcription activities. 5 out of 9 categories with the highest Normalized Enrichment Scores are shown where $p_{adjusted}$ <0.05. Categories not shown had highly overlapping gene sets with those that are highlighted. **D** Western blots show that transcription factors FOSB and JUN are increased due to 2-5A activation. Different FOSB isoforms are marked with black arrows. **E** Western blots show JNK and p38 are activated in A549 cells after 2-5A treatment. Different JNK isoforms are marked with black arrows. ZAKα is hyperphosphorylated during RNase L activation. Upper bar shows phosphorylated ZAKα in a Phos-Tag gel (shifted from its expected molecular weight). Lower line points to non-phosphorylated ZAKα. **F** Working model of JNK/p38 pathway activation by RNase L. RNase L cleaves mRNAs that are being translated. At the end of the resulting fragments, ribosomes can collide and activate ZAKα and subsequently JNK and p38.

Figure 2. *OAS-RNase L and other dsRNA pathways act together to induce the proinflammatory response.* **A** Schematics of RNA-seq experiments. A549 cells were transfected with poly I:C (leading to activation of MDA5, RIG-I, and PKR, besides OAS). **B** Venn-diagram showing the overlap of DE genes in cells treated with poly I:C in WT (magenta), 2-5A in WT (yellow) and poly I:C in *RNASEL* KO cells (green, abbreviated to KO). **C** Correlation between differential expression changes in 2-5A (activation of RNase L) vs poly I:C (activation of all dsRNA pathways including RNase L) treated cells. Blue and red dots represent JNK/p38 MAPK activation-related or IFN stimulated genes (as

875 defined in Materials and Methods), differentially expressed in 2-5A or poly I:C treated
876 cells, respectively. Black dot represents *GADD34*. **D** Violin plot representation of genes
877 related to JNK and p38 MAPK activation and interferon stimulation. Statistical testing
878 (paired t-tests) showed significant differences between data sets as indicated (p value
879 <0.001, marked by ***). **E** Effects of activating the OAS-RNase L pathway on
880 phosphorylation of JNK, p38, eIF2α and IRF3 assayed by Western blotting. ZAKα is
881 hyperphosphorylated during dsRNA response. Upper bar shows phosphorylated ZAKα in
882 a Phos-Tag gel (shifted from its expected molecular weight). Lower line points to non-
883 phosphorylated ZAKα. **F** Quantification of western blot for poly I:C treated WT and
884 *RNASEL* KO cells to assess level of activation when RNase L is activated alone or with
885 other dsRNA pathways. Activation levels are normalized to that of poly I:C treated WT
886 cells. Data reveal strong RNase L dependence for JNK and some dependence for p38,
887 eIF2α, and IRF3. **G** Model for RNase L acting synergistically with the other dsRNA
888 pathways to enhance the antiviral effect for JNK and p38 via ZAKα.
889
890 **Figure 3.** *Global RNA cleavage in the cell leads to transcriptional changes.* **A** Schematics
891 of RNA-seq experiments. *RNASEL* KO A549 cells were electroporated with RNase A or
892 BSA (control) and RNA-seq experiments were performed as described in Materials and
893 Methods. **B** Venn-diagram showing the number of upregulated genes (defined as $p_{adjusted}$
894 value <0.05 and log2fold changes >1) in RNase A electroporated samples (purple) and
895 2-5A treated cells (yellow). **C** Comparison of RNA log2 fold changes between RNase L
896 activated vs RNase A electroporated samples. Blue dots are representing transcripts
897 related to JNK and p38 activation. **D** Violin plot representation of those genes related to
898 JNK and p38 activation (*N* = 54, as defined in Materials and Methods) in RNase A
899 electroporated cells. *RNASEL* KO is abbreviated to KO. Statistical analysis (paired t-test)
900 showed that the log2 fold changes between RNase A electroporated and 2-5A activated
901 samples were not significantly different ($p_{adjusted}$ value >0.05, marked by n.s.). **E** JNK, p38
902 and ZAKα are activated due to RNase A treatment, as shown by western blots. Different
903 JNK isoforms are marked with black arrows. Upper bar shows phosphorylated ZAKα in a
904 Phos-Tag gel (shifted from its expected molecular weight). Lower line points to non-
905 phosphorylated ZAKα.

906

907 **Figure 4.** *RNA fragmentation leads to alternative ORF (altORF) translation*. **A** Schematics
908 of ribosome profiling experiments. *RNASEL* KO A549 cells were electroporated with
909 RNase A or BSA (control) and ribosome profiling experiments were performed as
910 described in Materials and Methods. **B** Ribosome profiling reads in the 3'UTR of the
911 *ACTG1* gene model shows the signature of altORF translation in RNase A electroporated
912 and RNase L activated A549 cells, but not in the controls (-2-5A and BSA). **C** Increased
913 3'UTR:ORF ratios indicate higher fraction of translation in 3'UTRs when active RNases
914 are present in the cell, but not in controls (-2-5A and BSA). **D** Normalized average
915 ribosome footprint occupancy (metagene plot) around the stop codon of main ORFs (left
916 panel) reveals increased proportion of ribosome footprints in the 3' UTRs (right panel,
917 zoom in). **E** Increased 3'UTR:ORF ratios indicate altORF translation during thapsigargin
918 treatment and activation of the UPR, but not in untreated cells.
919 In all panels, data shown for RNase L activation (+2-5A) were obtained from [21].
920

921 **Figure 5.** *RNase L activation influences translational control and effects of poly I:C*
922 *treatment.* **A**. Comparison of changes in RNA-seq vs ribosome profiling under conditions
923 of 2-5A treated WT cells (left), poly I:C treated WT cells (center), and poly I:C treated
924 *RNASEL* KO A549 cells (right). To emphasize the highest and most significant changes,
925 genes were filtered for the following criteria: log2 fold changes >4 (either RNA-seq or
926 ribosome profiling), $p_{adjusted}$ <0.01, normalized mean counts across the samples >50 (see
927 Materials and Methods for details). Dotted diagonal lines represent TE changes >2 fold.
928 Orange circles represent genes encoded by the mitochondria. **B.** TEs from individual
929 replicates of representative genes with downregulated (*MUC5AC* and *MUC5B*) or
930 upregulated (*CXCL3* or *CXCL8*) translation were computed. TEs calculated as described
931 in Materials and Methods. *RNASEL* KO is abbreviated to KO in all panels.
932

933 **Figure 6.** *RNase L modulates elements of the Integrated Stress Response.* **A** Bar plots
934 representing TEs of *GADD34* mRNA during poly I:C treatment in WT and *RNASEL KO*
935 cells. These data show that TE changes are greater in *RNASEL* KO cells during the ISR
936 as compared to respective controls. **B** Ribosome profiling tracks of gene models for

937 *GADD34* (*PPP1R15A*) in WT and *RNASEL* KO cells during poly I:C treatment suggest a
938 change in 5'UTR vs main ORF translation ratio in *RNASEL* KO cells during the ISR as
939 compared to WT cells and their respective controls. **C** 5'UTR:main ORF ratios of ribosome
940 profiling data in WT and *RNASEL* KO cells with and without poly I:C treatment were
941 computed for individual replicates. Data show this value is more strongly reduced upon
942 poly I:C treatment in cells where RNase L is absent. **D.** Western blot for GADD34 shows
943 increased levels of protein in poly I:C treated *RNASEL* KO cells, reflecting both the lack
944 of mRNA degradation and enhanced TE in cells where RNase L is absent.
945
946 **Figure 7.** *IFIT mRNAs undergo changes in translation that depend on RNase L.* **A** uORFs
947 were identified on *IFIT1* mRNAs based on the increase in ribosomes density at alternative
948 start codons (CUG, green markings) in poly I:C treated cells. Red marking shows the start
949 codon of the main ORF. **B** TEs of *IFIT1-3* mRNAs are decreased in RNase L deficient
950 cells (comparing WT and *RNASEL* KO poly I:C treated cells) consistently across
951 replicates. **C** *IFIT1-3* mRNAs were found to have less 5'UTR relative to main ORF
952 translation in poly I:C treated *RNASEL* KO (abbreviated to KO) cells as compared to WT
953 cells. **D** Schematics of how eIF2α phosphorylation and activation of RNase L affects gene
954 expression in the cell. While both mechanisms lead to reduced gene expression (less
955 translation when eIF2α is phosphorylated and less overall mRNA when RNase L is
956 activated), eIF2α phosphorylation increases translation of *GADD34* but RNase L reduces
957 its translation. Similarly, RNase L reduces *IFIT* mRNA translation. It may also be
958 increased via uORF regulation under conditions of eIF2α phosphorylation (marked by
959 asterisk since further confirmation is needed).
960
961 **S1 Related to Figure 1. A** Cleavage patterns of total RNA extracts show activation of
962 RNase L in 2-5A or poly I:C treated WT, but not *RNASEL* KO, A549 cells. rRNA cleavage
963 assay performed on a BioAnalyzer. Black arrows indicate the 28 and 18S rRNAs and red
964 arrows show RNase L degradation products. **B** Heatmap representation of the most
965 highly expressed genes during RNase L activation. Trends are consistent across
966 replicates. **C** Western blots show that transcription factors FOSB and JUN do not increase
967 in *RNASEL* KO cell due to 2-5A activation. **D** Western blots show JNK, p38 and ZAKα

968 are not activated in *RNASEL* KO cells after 2-5A treatment. **E** Western blots show ERK
969 is not activated in WT cells after 2-5A treatment.
970
971 **S2 Related to Figure 2.** Western blots show no detectable effect of RNase L activation
972 on NF-κB activation by poly I:C and no detectable activation by 2-5A. ERK activation was
973 not observed during 2-5A or poly I:C treatment.
974
975 **S3 Related to Figure 3. A** Cleavage of RNAs in the cell occurs when RNase A is
976 electroporated into cells, but not when BSA is electroporated, as observed by rRNA
977 cleavage assays performed on BioAnalyzer. Arrows indicate the 28S and 18S rRNAs. **B**
978 Volcano plot showing upregulation of example proinflammatory cytokines and
979 transcription factors during RNase A electroporation. Differentially expressed genes
980 define as $p_{adjusted}$ value <0.05, log_2fold change >1.
981
982 **S4 Related to Figure 4. A** Increased 5'UTR:ORF ratios indicating higher relative uORF
983 translation when active RNase is present in the cell, but not in controls (-2-5A and BSA
984 electroporated). **B** Normalized average ribosome footprint occupancy (metagene plot)
985 around the start codon of main ORFs reveals increased relative ribosome footprint levels
986 in the 5' UTRs when an active RNase is present vs the respective control.
987 In all panels data shown for RNase L activation (+2-5A) was obtained from [21].
988
989 **S5 Related to Figure 6. A** Ribosome profiling tracks for gene model of *ATF4* and *CHOP*
990 in WT and *RNASEL* KO cells during 2-5A or poly I:C treatment. Data show the poly I:C
991 dependent shift toward main ORF vs 5'UTR translation is greater when RNase L is
992 absent. Asterisks show RNase L dependent ribosome profiling peaks in 2-5A and poly
993 I:C treated cells that likely correspond to altORF translation initiation events. **B**
994 5'UTR:main ORF ratios computed from ribosome profiling data in WT and *RNASEL* KO
995 cells during poly I:C treatment for *ATF4* and *CHOP*.
996
997 **S6 Related to Figure 7. A** uORFs were identified on *IFIT2* and *3* mRNAs based on the
998 increase in ribosome densities on alternative start codons (CUG or GUG, green markings)

999 in poly I:C treated WT or *RNASEL* KO cells. Red marking shows the start codon for the
1000 main ORF. **B** Western blot for *IFIT1* and *IFIT2* shows increased protein levels in poly I:C
1001 treated RNase L KO cells, suggesting control of TE or RNA degradation reduce levels in
1002 WT cells.
1003
1004 **Table S1.** Results tables from DESeq2 analysis for RNA-seq (WT and *RNASEL* KO, +/-
1005 2-5A, +/- poly I:C, BSA vs RNase A electroporated).
1006 **Table S2.** Results tables from DESeq2 analysis for ribosome profiling (WT and *RNASEL*
1007 KO, +/-2-5A, +/- poly I:C).
1008 **Table S3.** List of genes that are upregulated by JNK/p38 in WT 2-5A treated cells and
1009 interferon response in WT poly I:C treated cells. This list was used to create violin plots
1010 in Figures 2D and 3D. In addition, a longer list of all genes related to JNK/p38 or interferon
1011 are given, as derived from the Harmonizome and Hallmark datasets, respectively (see
1012 Methods), used in Figures 2C and 3C.
1013
1014
1015
1016
1017

1018 **References**

1019 1. Hartmann, G. (2017). Nucleic Acid Immunity. Advances in immunology *133*, 121-169.
1020 10.1016/bs.ai.2016.11.001.
1021 2. Banerjee, S., Li, G., Li, Y., Gaughan, C., Baskar, D., Parker, Y., Lindner, D.J., Weiss, S.R., and
1022 Silverman, R.H. (2015). RNase L is a negative regulator of cell migration. Oncotarget *6*,
1023 44360-44372. 10.18632/oncotarget.6246.
1024 3. Castelli, J.C., Hassel, B.A., Wood, K.A., Li, X.L., Amemiya, K., Dalakas, M.C., Torrence, P.F.,
1025 and Youle, R.J. (1997). A study of the interferon antiviral mechanism: apoptosis activation
1026 by the 2-5A system. The Journal of experimental medicine *186*, 967-972.
1027 10.1084/jem.186.6.967.
1028 4. Silverman, R.H. (2007). Viral encounters with 2',5'-oligoadenylate synthetase and RNase
1029 L during the interferon antiviral response. Journal of virology *81*, 12720-12729.
1030 10.1128/jvi.01471-07.
1031 5. Donovan, J., Rath, S., Kolet-Mandrikov, D., and Korennykh, A. (2017). Rapid RNase L-
1032 driven arrest of protein synthesis in the dsRNA response without degradation of
1033 translation machinery. RNA (New York, N.Y.) *23*, 1660-1671. 10.1261/rna.062000.117.
1034 6. Lee, T.Y., Ezelle, H.J., Venkataraman, T., Lapidus, R.G., Scheibner, K.A., and Hassel, B.A.
1035 (2013). Regulation of human RNase-L by the miR-29 family reveals a novel oncogenic role
1036 in chronic myelogenous leukemia. Journal of interferon & cytokine research : the official
1037 journal of the International Society for Interferon and Cytokine Research *33*, 34-42.
1038 10.1089/jir.2012.0062.
1039 7. Long, T.M., Chakrabarti, A., Ezelle, H.J., Brennan-Laun, S.E., Raufman, J.P., Polyakova, I.,
1040 Silverman, R.H., and Hassel, B.A. (2013). RNase-L deficiency exacerbates experimental
1041 colitis and colitis-associated cancer. Inflammatory bowel diseases *19*, 1295-1305.
1042 10.1097/MIB.0b013e318281f2fd.
1043 8. Carpten, J., Nupponen, N., Isaacs, S., Sood, R., Robbins, C., Xu, J., Faruque, M., Moses, T.,
1044 Ewing, C., Gillanders, E., et al. (2002). Germline mutations in the ribonuclease L gene in
1045 families showing linkage with HPC1. Nature genetics *30*, 181-184. 10.1038/ng823.
1046 9. Casey, G., Neville, P.J., Plummer, S.J., Xiang, Y., Krumroy, L.M., Klein, E.A., Catalona, W.J.,
1047 Nupponen, N., Carpten, J.D., Trent, J.M., et al. (2002). RNASEL Arg462Gln variant is
1048 implicated in up to 13% of prostate cancer cases. Nature genetics *32*, 581-583.
1049 10.1038/ng1021.
1050 10. Magg, T., Okano, T., Koenig, L.M., Boehmer, D.F.R., Schwartz, S.L., Inoue, K., Heimall, J.,
1051 Licciardi, F., Ley-Zaporozhan, J., Ferdman, R.M., et al. (2021). Heterozygous OAS1 gain-of-
1052 function variants cause an autoinflammatory immunodeficiency. Sci Immunol *6*.
1053 10.1126/sciimmunol.abf9564.
1054 11. Young, S.K., and Wek, R.C. (2016). Upstream Open Reading Frames Differentially Regulate
1055 Gene-specific Translation in the Integrated Stress Response. J Biol Chem *291*, 16927-
1056 16935. 10.1074/jbc.R116.733899.
1057 12. Hinnebusch, A.G., Ivanov, I.P., and Sonenberg, N. (2016). Translational control by 5'-
1058 untranslated regions of eukaryotic mRNAs. Science *352*, 1413-1416.
1059 10.1126/science.aad9868.

1060 13. Costa-Mattioli, M., and Walter, P. (2020). The integrated stress response: From
1061 mechanism to disease. Science *368*. 10.1126/science.aat5314.
1062 14. Malathi, K., Paranjape, J.M., Bulanova, E., Shim, M., Guenther-Johnson, J.M., Faber, P.W.,
1063 Eling, T.E., Williams, B.R., and Silverman, R.H. (2005). A transcriptional signaling pathway
1064 in the IFN system mediated by 2'-5'-oligoadenylate activation of RNase L. Proc Natl Acad
1065 Sci U S A *102*, 14533-14538. 10.1073/pnas.0507551102.
1066 15. Andersen, J.B., Mazan-Mamczarz, K., Zhan, M., Gorospe, M., and Hassel, B.A. (2009).
1067 Ribosomal protein mRNAs are primary targets of regulation in RNase-L-induced
1068 senescence. RNA biology *6*, 305-315. 10.4161/rna.6.3.8526.
1069 16. Rath, S., Prangley, E., Donovan, J., Demarest, K., Wingreen, N.S., Meir, Y., and Korennykh,
1070 A. (2019). Concerted 2-5A-Mediated mRNA Decay and Transcription Reprogram Protein
1071 Synthesis in the dsRNA Response. Molecular cell *75*, 1218-1228.e1216.
1072 10.1016/j.molcel.2019.07.027.
1073 17. Burke, J.M., Moon, S.L., Matheny, T., and Parker, R. (2019). RNase L Reprograms
1074 Translation by Widespread mRNA Turnover Escaped by Antiviral mRNAs. Molecular cell
1075 *75*, 1203-1217.e1205. 10.1016/j.molcel.2019.07.029.
1076 18. Malathi, K., Dong, B., Gale, M., Jr., and Silverman, R.H. (2007). Small self-RNA generated
1077 by RNase L amplifies antiviral innate immunity. Nature *448*, 816-819.
1078 10.1038/nature06042.
1079 19. Manivannan, P., Siddiqui, M.A., and Malathi, K. (2020). RNase L Amplifies Interferon
1080 Signaling by Inducing Protein Kinase R-Mediated Antiviral Stress Granules. Journal of
1081 virology *94*, e00205-00220. 10.1128/jvi.00205-20.
1082 20. Chakrabarti, A., Banerjee, S., Franchi, L., Loo, Y.M., Gale, M., Jr., Núñez, G., and Silverman,
1083 R.H. (2015). RNase L activates the NLRP3 inflammasome during viral infections. Cell Host
1084 Microbe *17*, 466-477. 10.1016/j.chom.2015.02.010.
1085 21. Karasik, A., Jones, G.D., DePass, A.V., and Guydosh, N.R. (2021). Activation of the antiviral
1086 factor RNase L triggers translation of non-coding mRNA sequences. Nucleic Acids Res *49*,
1087 6007-6026. 10.1093/nar/gkab036.
1088 22. Li, G., Xiang, Y., Sabapathy, K., and Silverman, R.H. (2004). An apoptotic signaling pathway
1089 in the interferon antiviral response mediated by RNase L and c-Jun NH2-terminal kinase.
1090 J Biol Chem *279*, 1123-1131. 10.1074/jbc.M305893200.
1091 23. Iordanov, M.S., Paranjape, J.M., Zhou, A., Wong, J., Williams, B.R., Meurs, E.F., Silverman,
1092 R.H., and Magun, B.E. (2000). Activation of p38 mitogen-activated protein kinase and c-
1093 Jun NH(2)-terminal kinase by double-stranded RNA and encephalomyocarditis virus:
1094 involvement of RNase L, protein kinase R, and alternative pathways. Mol Cell Biol *20*, 617-
1095 627. 10.1128/mcb.20.2.617-627.2000.
1096 24. Siddiqui, M.A., and Malathi, K. (2012). RNase L induces autophagy via c-Jun N-terminal
1097 kinase and double-stranded RNA-dependent protein kinase signaling pathways. J Biol
1098 Chem *287*, 43651-43664. 10.1074/jbc.M112.399964.
1099 25. Wu, C.C., Peterson, A., Zinshteyn, B., Regot, S., and Green, R. (2020). Ribosome Collisions
1100 Trigger General Stress Responses to Regulate Cell Fate. Cell *182*, 404-416.e414.
1101 10.1016/j.cell.2020.06.006.

1102 26. Vind, A.C., Genzor, A.V., and Bekker-Jensen, S. (2020). Ribosomal stress-surveillance:
1103 three pathways is a magic number. Nucleic Acids Res *48*, 10648-10661.
1104 10.1093/nar/gkaa757.
1105 27. Vind, A.C., Snieckute, G., Blasius, M., Tiedje, C., Krogh, N., Bekker-Jensen, D.B., Andersen,
1106 K.L., Nordgaard, C., Tollenaere, M.A.X., Lund, A.H., et al. (2020). ZAKα Recognizes Stalled
1107 Ribosomes through Partially Redundant Sensor Domains. Molecular cell *78*, 700-
1108 713.e707. 10.1016/j.molcel.2020.03.021.
1109 28. Robinson, K.S., Toh, G.A., Rozario, P., Chua, R., Bauernfried, S., Sun, Z., Firdaus, M.J.,
1110 Bayat, S., Nadkarni, R., Poh, Z.S., et al. (2022). ZAKα-driven ribotoxic stress response
1111 activates the human NLRP1 inflammasome. Science *377*, 328-335.
1112 10.1126/science.abl6324.
1113 29. Guydosh, N.R., Kimmig, P., Walter, P., and Green, R. (2017). Regulated Ire1-dependent
1114 mRNA decay requires no-go mRNA degradation to maintain endoplasmic reticulum
1115 homeostasis in S. pombe. Elife *6*. 10.7554/eLife.29216.
1116 30. Floyd-Smith, G., Slattery, E., and Lengyel, P. (1981). Interferon action: RNA cleavage
1117 pattern of a (2'-5')oligoadenylate--dependent endonuclease. Science *212*, 1030-1032.
1118 10.1126/science.6165080.
1119 31. Love, M.I., Huber, W., and Anders, S. (2014). Moderated estimation of fold change and
1120 dispersion for RNA-seq data with DESeq2. Genome Biol *15*, 550. 10.1186/s13059-014-
1121 0550-8.
1122 32. Rath, S., Donovan, J., Whitney, G., Chitrakar, A., Wang, W., and Korennykh, A. (2015).
1123 Human RNase L tunes gene expression by selectively destabilizing the microRNA-
1124 regulated transcriptome. Proc Natl Acad Sci U S A *112*, 15916-15921.
1125 10.1073/pnas.1513034112.
1126 33. Dhanasekaran, D.N., and Reddy, E.P. (2017). JNK-signaling: A multiplexing hub in
1127 programmed cell death. Genes Cancer *8*, 682-694. 10.18632/genesandcancer.155.
1128 34. Dalet, A., Argüello, R.J., Combes, A., Spinelli, L., Jaeger, S., Fallet, M., Vu Manh, T.P.,
1129 Mendes, A., Perego, J., Reverendo, M., et al. (2017). Protein synthesis inhibition and
1130 GADD34 control IFN-β heterogeneous expression in response to dsRNA. Embo j *36*, 761-
1131 782. 10.15252/embj.201695000.
1132 35. Burke, J.M., Gilchrist, A.R., Sawyer, S.L., and Parker, R. (2021). RNase L limits host and viral
1133 protein synthesis via inhibition of mRNA export. Sci Adv *7*. 10.1126/sciadv.abh2479.
1134 36. Bisbal, C., Martinand, C., Silhol, M., Lebleu, B., and Salehzada, T. (1995). Cloning and
1135 characterization of a RNAse L inhibitor. A new component of the interferon-regulated 2-
1136 5A pathway. J Biol Chem *270*, 13308-13317.
1137 37. Le Roy, F., Salehzada, T., Bisbal, C., Dougherty, J.P., and Peltz, S.W. (2005). A newly
1138 discovered function for RNase L in regulating translation termination. Nat Struct Mol Biol
1139 *12*, 505-512. 10.1038/nsmb944.
1140 38. Nogimori, T., Nishiura, K., Kawashima, S., Nagai, T., Oishi, Y., Hosoda, N., Imataka, H.,
1141 Kitamura, Y., Kitade, Y., and Hoshino, S.I. (2019). Dom34 mediates targeting of exogenous
1142 RNA in the antiviral OAS/RNase L pathway. Nucleic Acids Res *47*, 432-449.
1143 10.1093/nar/gky1087.

1144 39. Nogimori, T., Ogami, K., Oishi, Y., Goda, R., Hosoda, N., Kitamura, Y., Kitade, Y., and
1145 Hoshino, S.I. (2020). ABCE1 Acts as a Positive Regulator of Exogenous RNA Decay. Viruses
1146 *12*. 10.3390/v12020174.
1147 40. Tnani, M., Aliau, S., and Bayard, B. (1998). Localization of a molecular form of interferon-
1148 regulated RNase L in the cytoskeleton. Journal of interferon & cytokine research : the
1149 official journal of the International Society for Interferon and Cytokine Research *18*, 361-
1150 368. 10.1089/jir.1998.18.361.
1151 41. Nogués, M.V., Vilanova, M., and Cuchillo, C.M. (1995). Bovine pancreatic ribonuclease A
1152 as a model of an enzyme with multiple substrate binding sites. Biochim Biophys Acta
1153 *1253*, 16-24. 10.1016/0167-4838(95)00138-k.
1154 42. Borkakoti, N. (1983). Enzyme specificity: base recognition and hydrolysis of RNA by
1155 ribonuclease A. FEBS Lett *162*, 367-373. 10.1016/0014-5793(83)80789-3.
1156 43. Walter, P., and Ron, D. (2011). The unfolded protein response: from stress pathway to
1157 homeostatic regulation. Science *334*, 1081-1086. 10.1126/science.1209038.
1158 44. Hollien, J., Lin, J.H., Li, H., Stevens, N., Walter, P., and Weissman, J.S. (2009). Regulated
1159 Ire1-dependent decay of messenger RNAs in mammalian cells. J Cell Biol *186*, 323-331.
1160 10.1083/jcb.200903014.
1161 45. Woo, Y.M., Kwak, Y., Namkoong, S., Kristjánsdóttir, K., Lee, S.H., Lee, J.H., and Kwak, H.
1162 (2018). TED-Seq Identifies the Dynamics of Poly(A) Length during ER Stress. Cell Rep *24*,
1163 3630-3641.e3637. 10.1016/j.celrep.2018.08.084.
1164 46. Dai, A., Cao, S., Dhungel, P., Luan, Y., Liu, Y., Xie, Z., and Yang, Z. (2017). Ribosome Profiling
1165 Reveals Translational Upregulation of Cellular Oxidative Phosphorylation mRNAs during
1166 Vaccinia Virus-Induced Host Shutoff. Journal of virology *91*. 10.1128/jvi.01858-16.
1167 47. Wek, R.C., Jiang, H.Y., and Anthony, T.G. (2006). Coping with stress: eIF2 kinases and
1168 translational control. Biochem Soc Trans *34*, 7-11. 10.1042/bst20060007.
1169 48. Novoa, I., Zeng, H., Harding, H.P., and Ron, D. (2001). Feedback inhibition of the unfolded
1170 protein response by GADD34-mediated dephosphorylation of eIF2alpha. J Cell Biol *153*,
1171 1011-1022. 10.1083/jcb.153.5.1011.
1172 49. Fusakio, M.E., Willy, J.A., Wang, Y., Mirek, E.T., Al Baghdadi, R.J., Adams, C.M., Anthony,
1173 T.G., and Wek, R.C. (2016). Transcription factor ATF4 directs basal and stress-induced
1174 gene expression in the unfolded protein response and cholesterol metabolism in the liver.
1175 Mol Biol Cell *27*, 1536-1551. 10.1091/mbc.E16-01-0039.
1176 50. Ma, Y., Brewer, J.W., Diehl, J.A., and Hendershot, L.M. (2002). Two distinct stress signaling
1177 pathways converge upon the CHOP promoter during the mammalian unfolded protein
1178 response. J Mol Biol *318*, 1351-1365. 10.1016/s0022-2836(02)00234-6.
1179 51. Ma, Y., and Hendershot, L.M. (2003). Delineation of a negative feedback regulatory loop
1180 that controls protein translation during endoplasmic reticulum stress. J Biol Chem *278*,
1181 34864-34873. 10.1074/jbc.M301107200.
1182 52. Dever, T.E., Ivanov, I.P., and Hinnebusch, A.G. (2023). Translational regulation by uORFs
1183 and start codon selection stringency. Genes Dev *37*, 474-489. 10.1101/gad.350752.123.
1184 53. Fensterl, V., and Sen, G.C. (2015). Interferon-induced Ifit proteins: their role in viral
1185 pathogenesis. Journal of virology *89*, 2462-2468. 10.1128/jvi.02744-14.
1186 54. Iordanov, M.S., Pribnow, D., Magun, J.L., Dinh, T.H., Pearson, J.A., Chen, S.L., and Magun,
1187 B.E. (1997). Ribotoxic stress response: activation of the stress-activated protein kinase

1188 JNK1 by inhibitors of the peptidyl transferase reaction and by sequence-specific RNA
1189 damage to the alpha-sarcin/ricin loop in the 28S rRNA. Mol Cell Biol *17*, 3373-3381.
1190 10.1128/mcb.17.6.3373.
1191 55. Wang, X., Mader, M.M., Toth, J.E., Yu, X., Jin, N., Campbell, R.M., Smallwood, J.K., Christe,
1192 M.E., Chatterjee, A., Goodson, T., Jr., et al. (2005). Complete inhibition of anisomycin and
1193 UV radiation but not cytokine induced JNK and p38 activation by an aryl-substituted
1194 dihydropyrrolopyrazole quinoline and mixed lineage kinase 7 small interfering RNA. J Biol
1195 Chem *280*, 19298-19305. 10.1074/jbc.M413059200.
1196 56. Hartenian, E., and Glaunsinger, B.A. (2019). Feedback to the central dogma: cytoplasmic
1197 mRNA decay and transcription are interdependent processes. Crit Rev Biochem Mol Biol
1198 *54*, 385-398. 10.1080/10409238.2019.1679083.
1199 57. Wolin, S.L., and Walter, P. (1988). Ribosome pausing and stacking during translation of a
1200 eukaryotic mRNA. Embo j *7*, 3559-3569. 10.1002/j.1460-2075.1988.tb03233.x.
1201 58. Sundaramoorthy, E., Ryan, A.P., Fulzele, A., Leonard, M., Daugherty, M.D., and Bennett,
1202 E.J. (2021). Ribosome quality control activity potentiates vaccinia virus protein synthesis
1203 during infection. J Cell Sci *134*. 10.1242/jcs.257188.
1204 59. Müller, M.B.D., Kasturi, P., Jayaraj, G.G., and Hartl, F.U. (2023). Mechanisms of
1205 readthrough mitigation reveal principles of GCN1-mediated translational quality control.
1206 Cell *186*, 3227-3244.e3220. 10.1016/j.cell.2023.05.035.
1207 60. Snieckute, G., Genzor, A.V., Vind, A.C., Ryder, L., Stoneley, M., Chamois, S., Dreos, R.,
1208 Nordgaard, C., Sass, F., Blasius, M., et al. (2022). Ribosome stalling is a signal for metabolic
1209 regulation by the ribotoxic stress response. Cell Metab *34*, 2036-2046.e2038.
1210 10.1016/j.cmet.2022.10.011.
1211 61. Wickenhagen, A., Sugrue, E., Lytras, S., Kuchi, S., Noerenberg, M., Turnbull, M.L., Loney,
1212 C., Herder, V., Allan, J., Jarmson, I., et al. (2021). A prenylated dsRNA sensor protects
1213 against severe COVID-19. Science *374*, eabj3624. 10.1126/science.abj3624.
1214 62. Banday, A.R., Stanifer, M.L., Florez-Vargas, O., Onabajo, O.O., Papenberg, B.W., Zahoor,
1215 M.A., Mirabello, L., Ring, T.J., Lee, C.H., Albert, P.S., et al. (2022). Genetic regulation of
1216 OAS1 nonsense-mediated decay underlies association with COVID-19 hospitalization in
1217 patients of European and African ancestries. Nature genetics *54*, 1103-1116.
1218 10.1038/s41588-022-01113-z.
1219 63. Meydan, S., and Guydosh, N.R. (2020). Disome and Trisome Profiling Reveal Genome-
1220 wide Targets of Ribosome Quality Control. Molecular cell *79*, 588-602.e586.
1221 10.1016/j.molcel.2020.06.010.
1222 64. Yan, L.L., and Zaher, H.S. (2021). Ribosome quality control antagonizes the activation of
1223 the integrated stress response on colliding ribosomes. Molecular cell *81*, 614-628.e614.
1224 10.1016/j.molcel.2020.11.033.
1225 65. Pochopien, A.A., Beckert, B., Kasvandik, S., Berninghausen, O., Beckmann, R., Tenson, T.,
1226 and Wilson, D.N. (2021). Structure of Gcn1 bound to stalled and colliding 80S ribosomes.
1227 Proc Natl Acad Sci U S A *118*. 10.1073/pnas.2022756118.
1228 66. Fisher, T., Gluck, A., Narayanan, K., Kuroda, M., Nachshon, A., Hsu, J.C., Halfmann, P.J.,
1229 Yahalom-Ronen, Y., Tamir, H., Finkel, Y., et al. (2022). Parsing the role of NSP1 in SARS-
1230 CoV-2 infection. Cell Rep *39*, 110954. 10.1016/j.celrep.2022.110954.

1231 67. Thoms, M., Buschauer, R., Ameismeier, M., Koepke, L., Denk, T., Hirschenberger, M.,
1232 Kratzat, H., Hayn, M., Mackens-Kiani, T., Cheng, J., et al. (2020). Structural basis for
1233 translational shutdown and immune evasion by the Nsp1 protein of SARS-CoV-2. Science
1234 *369*, 1249-1255. 10.1126/science.abc8665.
1235 68. Mills, E.W., and Green, R. (2017). Ribosomopathies: There's strength in numbers. Science
1236 *358*. 10.1126/science.aan2755.
1237 69. Lodish, H.F. (1974). Model for the regulation of mRNA translation applied to haemoglobin
1238 synthesis. Nature *251*, 385-388. 10.1038/251385a0.
1239 70. Gaikwad, S., Ghobakhlou, F., Young, D.J., Visweswaraiah, J., Zhang, H., and Hinnebusch,
1240 A.G. (2021). Reprogramming of translation in yeast cells impaired for ribosome recycling
1241 favors short, efficiently translated mRNAs. Elife *10*. 10.7554/eLife.64283.
1242 71. Mills, E.W., Wangen, J., Green, R., and Ingolia, N.T. (2016). Dynamic Regulation of a
1243 Ribosome Rescue Pathway in Erythroid Cells and Platelets. Cell Rep *17*, 1-10.
1244 10.1016/j.celrep.2016.08.088.
1245 72. Lee, D., Le Pen, J., Yatim, A., Dong, B., Aquino, Y., Ogishi, M., Pescarmona, R., Talouarn, E.,
1246 Rinchai, D., Zhang, P., et al. (2023). Inborn errors of OAS–RNase L in SARS-CoV-
1247 2–related multisystem inflammatory syndrome in children. Science *0*, eabo3627.
1248 doi:10.1126/science.abo3627.
1249 73. Poe, J.C., Kountikov, E.I., Lykken, J.M., Natarajan, A., Marchuk, D.A., and Tedder, T.F.
1250 (2014). EndoU is a novel regulator of AICD during peripheral B cell selection. The Journal
1251 of experimental medicine *211*, 57-69. 10.1084/jem.20130648.
1252 74. Deng, X., and Baker, S.C. (2018). An "Old" protein with a new story: Coronavirus
1253 endoribonuclease is important for evading host antiviral defenses. Virology *517*, 157-163.
1254 10.1016/j.virol.2017.12.024.
1255 75. Siraj, Y.A. (2022). Promises of eukaryotic ribonucleases for cancer treatment: a systematic
1256 review. Translational Medicine Communications *7*, 5. 10.1186/s41231-022-00113-9.
1257 76. Mitkevich, V.A., Petrushanko, I.Y., and Makarov, A.A. (2019). RNases Disrupt the Adaptive
1258 Potential of Malignant Cells: Perspectives for Therapy. Front Pharmacol *10*, 922.
1259 10.3389/fphar.2019.00922.
1260 77. Liu, R., and Moss, B. (2016). Opposing Roles of Double-Stranded RNA Effector Pathways
1261 and Viral Defense Proteins Revealed with CRISPR-Cas9 Knockout Cell Lines and Vaccinia
1262 Virus Mutants. Journal of virology *90*, 7864-7879. 10.1128/jvi.00869-16.
1263 78. Langmead, B., Trapnell, C., Pop, M., and Salzberg, S.L. (2009). Ultrafast and memory-
1264 efficient alignment of short DNA sequences to the human genome. Genome Biol *10*, R25.
1265 10.1186/gb-2009-10-3-r25.
1266 79. Dobin, A., Davis, C.A., Schlesinger, F., Drenkow, J., Zaleski, C., Jha, S., Batut, P., Chaisson,
1267 M., and Gingeras, T.R. (2013). STAR: ultrafast universal RNA-seq aligner. Bioinformatics
1268 *29*, 15-21. 10.1093/bioinformatics/bts635.
1269 80. Picard toolkit. Broad Institute, GitHub repository
1270 https://broadinstitute.github.io/picard/.
1271 81. Liao, Y., Smyth, G.K., and Shi, W. (2014). featureCounts: an efficient general purpose
1272 program for assigning sequence reads to genomic features. Bioinformatics *30*, 923-930.
1273 10.1093/bioinformatics/btt656.

1274 82. Ramírez, F., Dündar, F., Diehl, S., Grüning, B.A., and Manke, T. (2014). deepTools: a flexible
1275 platform for exploring deep-sequencing data. Nucleic Acids Res *42*, W187-191.
1276 10.1093/nar/gku365.
1277 83. Yu, G., Wang, L.G., Han, Y., and He, Q.Y. (2012). clusterProfiler: an R package for
1278 comparing biological themes among gene clusters. Omics *16*, 284-287.
1279 10.1089/omi.2011.0118.
1280 84. Rouillard, A.D., Gundersen, G.W., Fernandez, N.F., Wang, Z., Monteiro, C.D., McDermott,
1281 M.G., and Ma'ayan, A. (2016). The harmonizome: a collection of processed datasets
1282 gathered to serve and mine knowledge about genes and proteins. Database (Oxford)
1283 *2016*. 10.1093/database/baw100.
1284 85. Liberzon, A., Birger, C., Thorvaldsdóttir, H., Ghandi, M., Mesirov, J.P., and Tamayo, P.
1285 (2015). The Molecular Signatures Database (MSigDB) hallmark gene set collection. Cell
1286 Syst *1*, 417-425. 10.1016/j.cels.2015.12.004.
1287 86. Guydosh, N.R. (2021). ribofootPrinter: A precision python toolbox for analysis of ribosome
1288 profiling data. bioRxiv.
1289 87. Schindelin, J., Arganda-Carreras, I., Frise, E., Kaynig, V., Longair, M., Pietzsch, T., Preibisch,
1290 S., Rueden, C., Saalfeld, S., Schmid, B., et al. (2012). Fiji: an open-source platform for
1291 biological-image analysis. Nat Methods *9*, 676-682. 10.1038/nmeth.2019.
1292

Figure 1

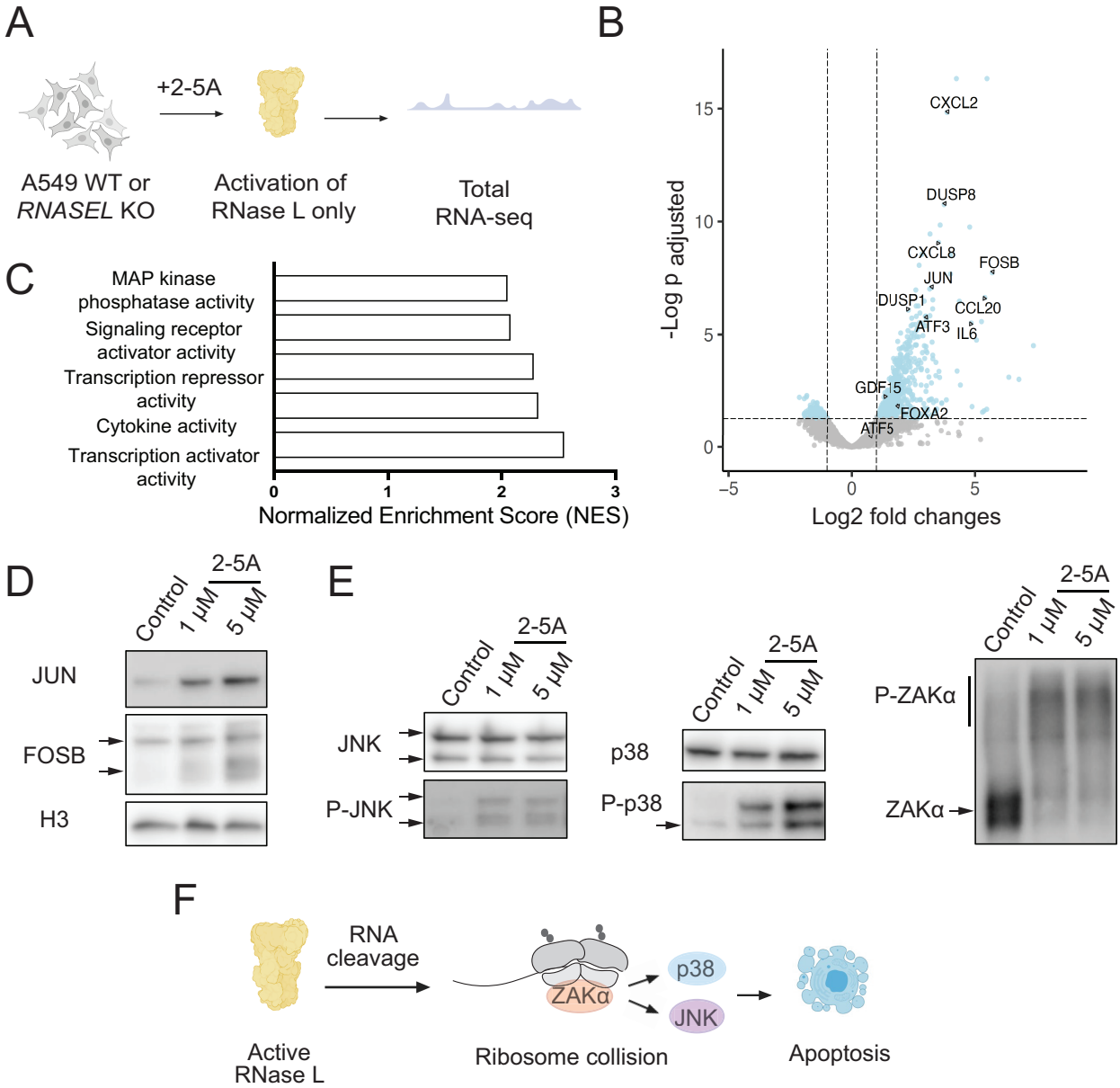
A
+2-5A
A549 WT or
RNASEL KO
Activation of
RNase L only
Total
RNA-seq
B
-Log p adjusted
Log2 fold changes
CXCL2
DUSP8
CXCL8
FOSB
JUN
DUSP1
CCL20
ATF3
IL6
GDF15
FOXA2
ATF5
C
MAP kinase
phosphatase activity
Signaling receptor
activator activity
Transcription repressor
activity
Cytokine activity
Transcription activator
activity
Normalized Enrichment Score (NES)
D
Control
2-5A
1 μM
5 μM
JUN
FOSB
H3
E
JNK
P-JNK
p38
P-p38
P-ZAKα
ZAKα
F
RNA
cleavage
ZAKα
p38
JNK
Active
RNase L
Ribosome collision
Apoptosis

Figure 2

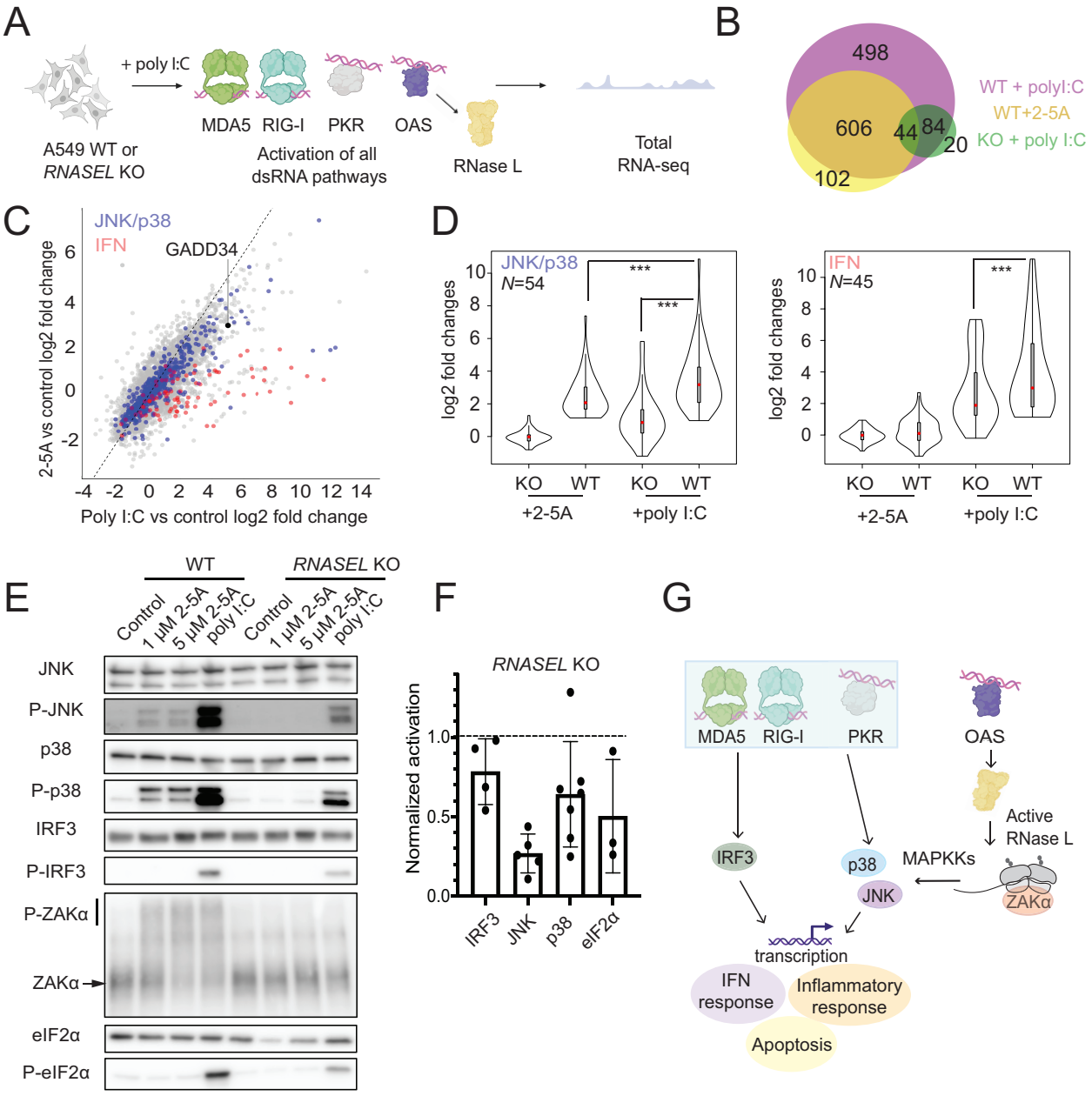
A
+ poly I:C
A549 WT or
RNASEL KO
MDA5
RIG-I
PKR
OAS
Activation of all
dsRNA pathways
RNase L
Total
RNA-seq
B
498
606
44
84
20
102
WT + polyI:C
WT+2-5A
KO + poly I:C
C
JNK/p38
IFN
GADD34
2-5A vs control log2 fold change
Poly I:C vs control log2 fold change
D
JNK/p38
N=54
IFN
N=45
log2 fold changes
***
KO
WT
+2-5A
+poly I:C
E
WT
RNASEL KO
Control
1 μM 2-5A
5 μM 2-5A
poly I:C
JNK
P-JNK
p38
P-p38
IRF3
P-IRF3
P-ZAKα
ZAKα
eIF2α
P-eIF2α
F
RNASEL KO
Normalized activation
IRF3
JNK
p38
eIF2α
G
MDA5
RIG-I
PKR
OAS
Active
RNase L
IRF3
p38
JNK
MAPKKs
ZAKα
transcription
IFN
response
Inflammatory
response
Apoptosis

Figure 3

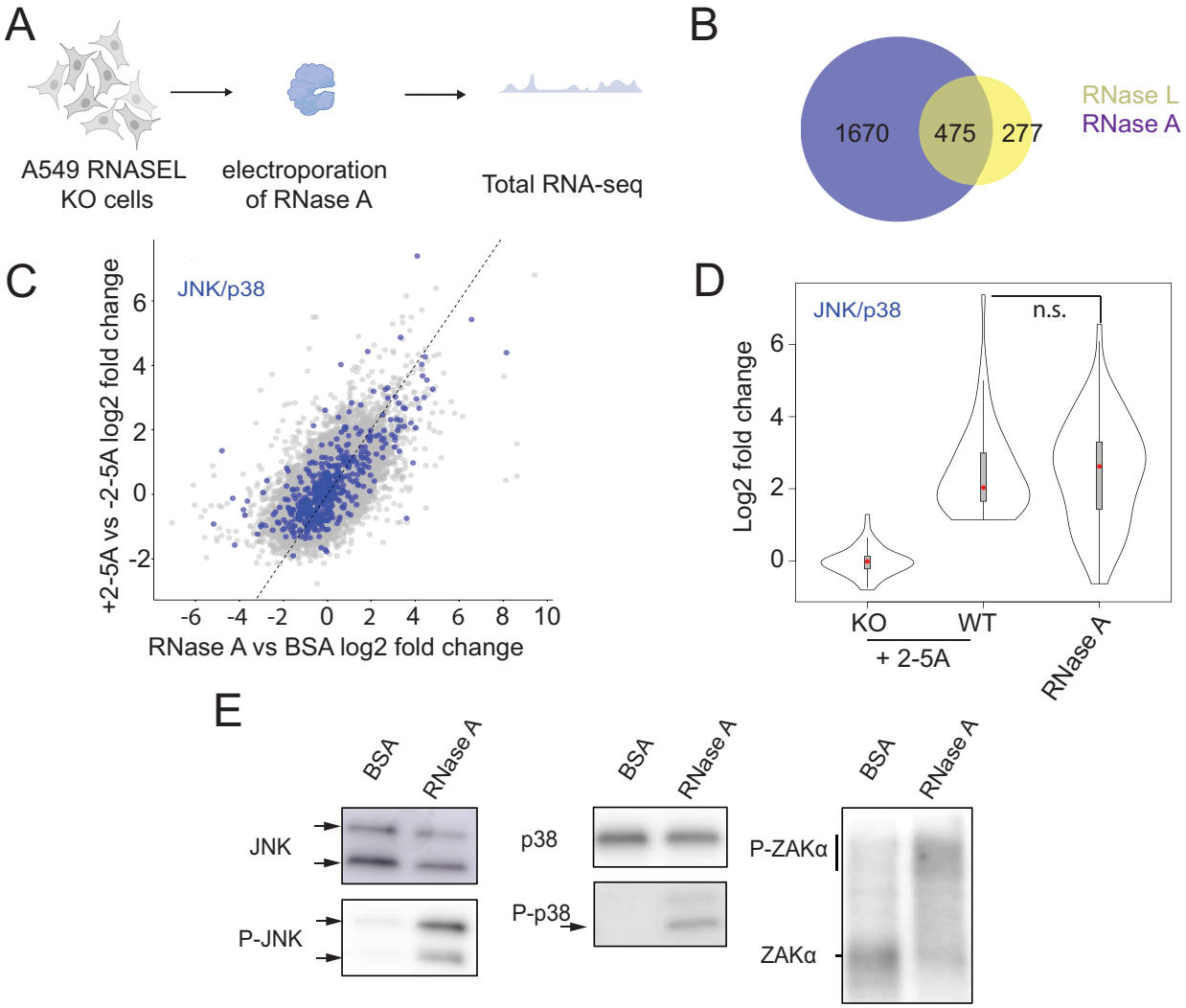
A
A549 RNASEL KO cells
electroporation of RNase A
Total RNA-seq
B
1670
475
277
RNase L
RNase A
C
JNK/p38
+2-5A vs -2-5A log2 fold change
RNase A vs BSA log2 fold change
D
JNK/p38
n.s.
Log2 fold change
KO
WT
+ 2-5A
RNase A
E
BSA
RNase A
JNK
P-JNK
p38
P-p38
P-ZAKα
ZAKα

Figure 4

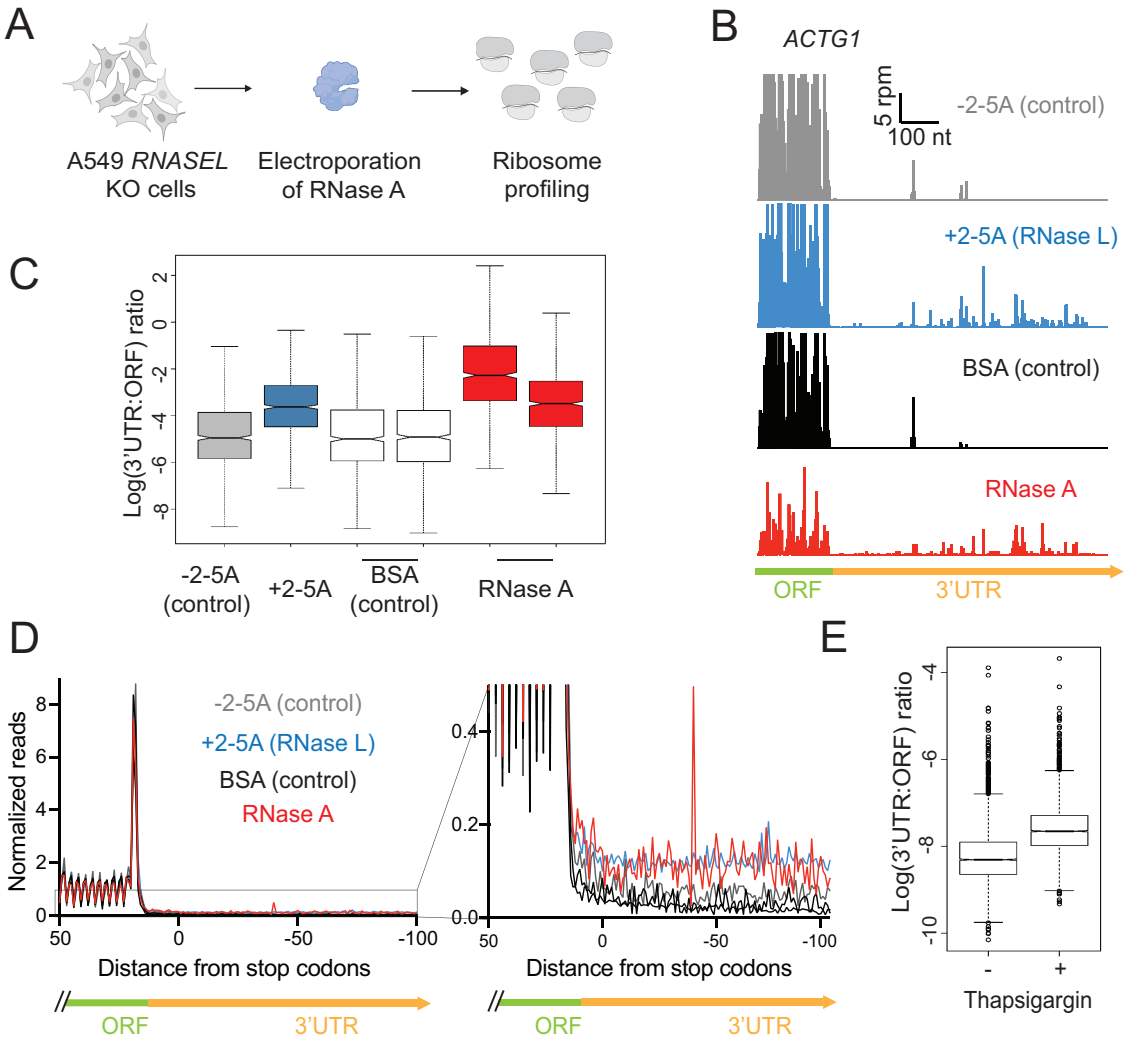
A
A549 RNASEL KO cells
Electroporation of RNase A
Ribosome profiling
B
ACTG1
5 rpm
100 nt
-2-5A (control)
+2-5A (RNase L)
BSA (control)
RNase A
ORF
3'UTR
C
Log(3'UTR:ORF) ratio
-2-5A (control)
+2-5A
BSA (control)
RNase A
D
Normalized reads
-2-5A (control)
+2-5A (RNase L)
BSA (control)
RNase A
Distance from stop codons
ORF
3'UTR
E
Log(3'UTR:ORF) ratio
Thapsigargin

Figure 5

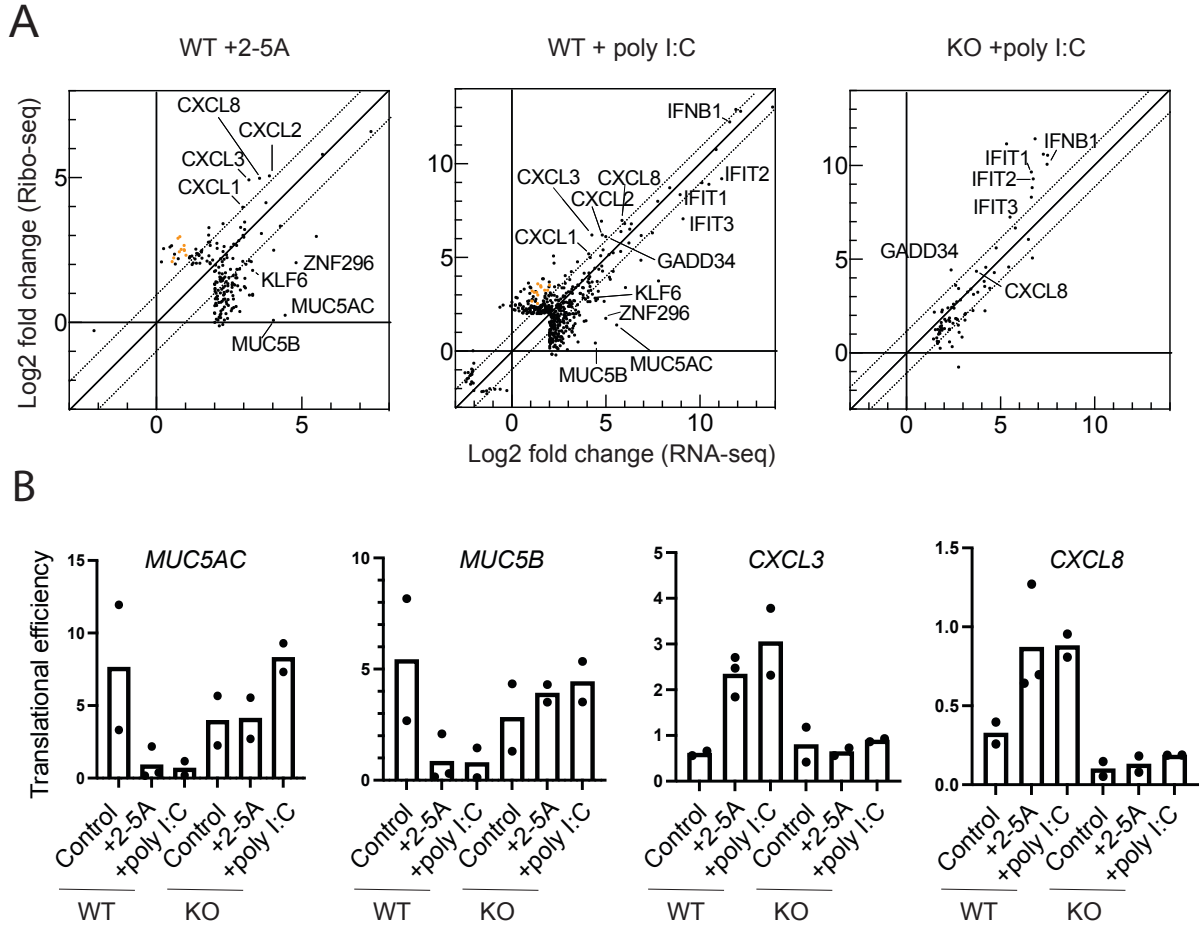
A
WT +2-5A
WT + poly I:C
KO +poly I:C
Log2 fold change (Ribo-seq)
Log2 fold change (RNA-seq)
CXCL8
CXCL2
CXCL3
CXCL1
ZNF296
KLF6
MUC5AC
MUC5B
IFNB1
IFIT2
IFIT1
IFIT3
GADD34
B
MUC5AC
MUC5B
CXCL3
CXCL8
Translational efficiency
Control
+2-5A
+poly I:C
WT
KO

Figure 6

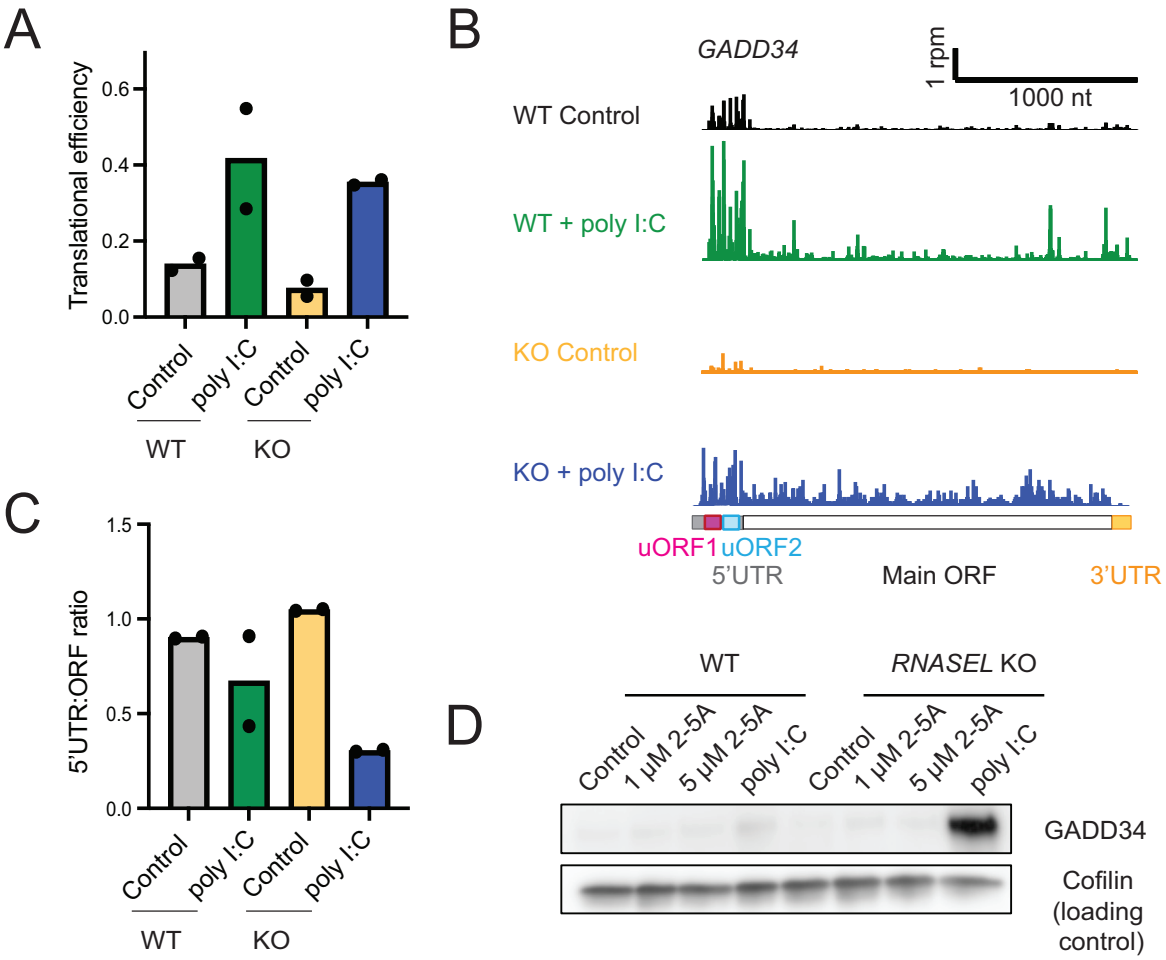
A
Translational efficiency
0.6
0.4
0.2
0.0
Control
poly I:C
Control
poly I:C
WT
KO
B
GADD34
1 rpm
1000 nt
WT Control
WT + poly I:C
KO Control
KO + poly I:C
uORF1
uORF2
5'UTR
Main ORF
3'UTR
C
5'UTR:ORF ratio
1.5
1.0
0.5
0.0
Control
poly I:C
Control
poly I:C
WT
KO
D
WT
RNASEL KO
Control
1 μM 2-5A
5 μM 2-5A
poly I:C
Control
1 μM 2-5A
5 μM 2-5A
poly I:C
GADD34
Cofilin
(loading
control)

Figure 7

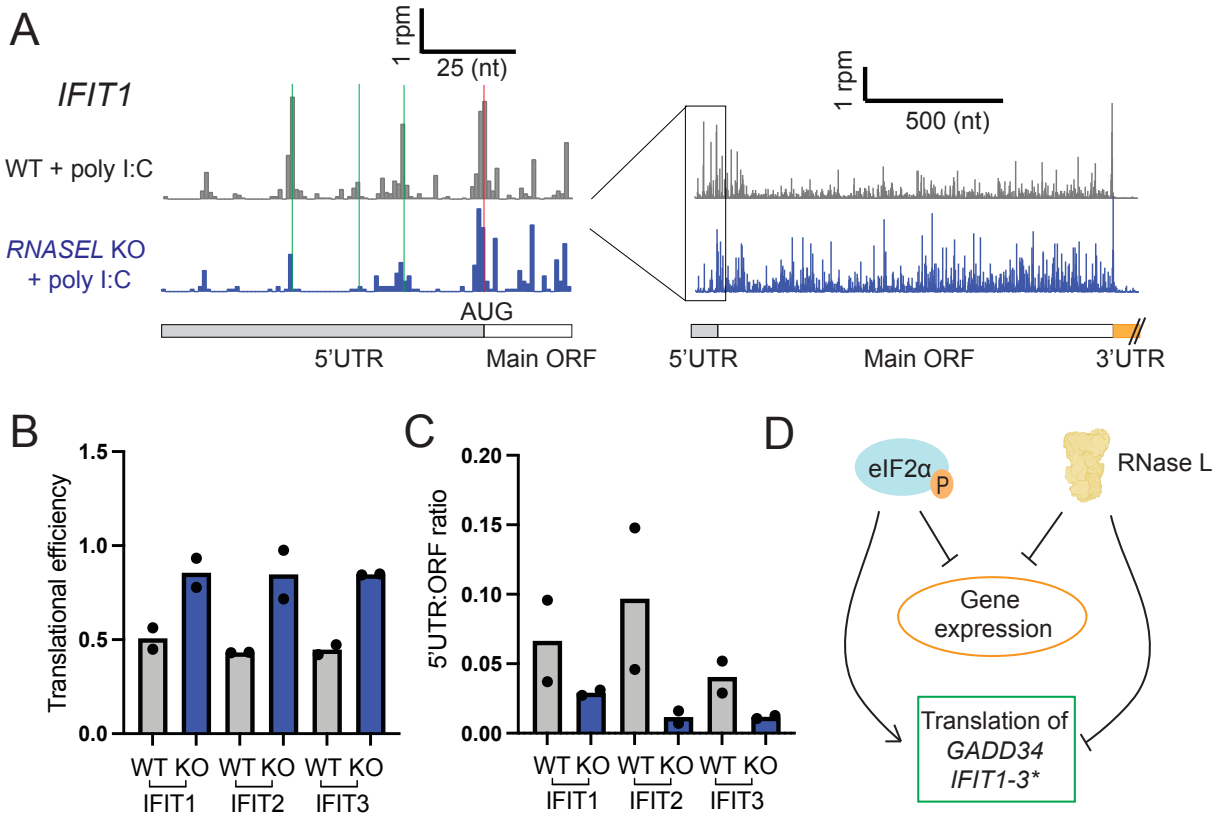
A
IFIT1
WT + poly I:C
RNASEL KO
+ poly I:C
1 rpm
25 (nt)
AUG
5'UTR
Main ORF
1 rpm
500 (nt)
5'UTR
Main ORF
3'UTR
B
Translational efficiency
1.5
1.0
0.5
0.0
WT KO WT KO WT KO
IFIT1 IFIT2 IFIT3
C
5'UTR:ORF ratio
0.20
0.15
0.10
0.05
0.00
WT KO WT KO WT KO
IFIT1 IFIT2 IFIT3
D
eIF2α
P
RNase L
Gene
expression
Translation of
GADD34
IFIT1-3*

Figure S1

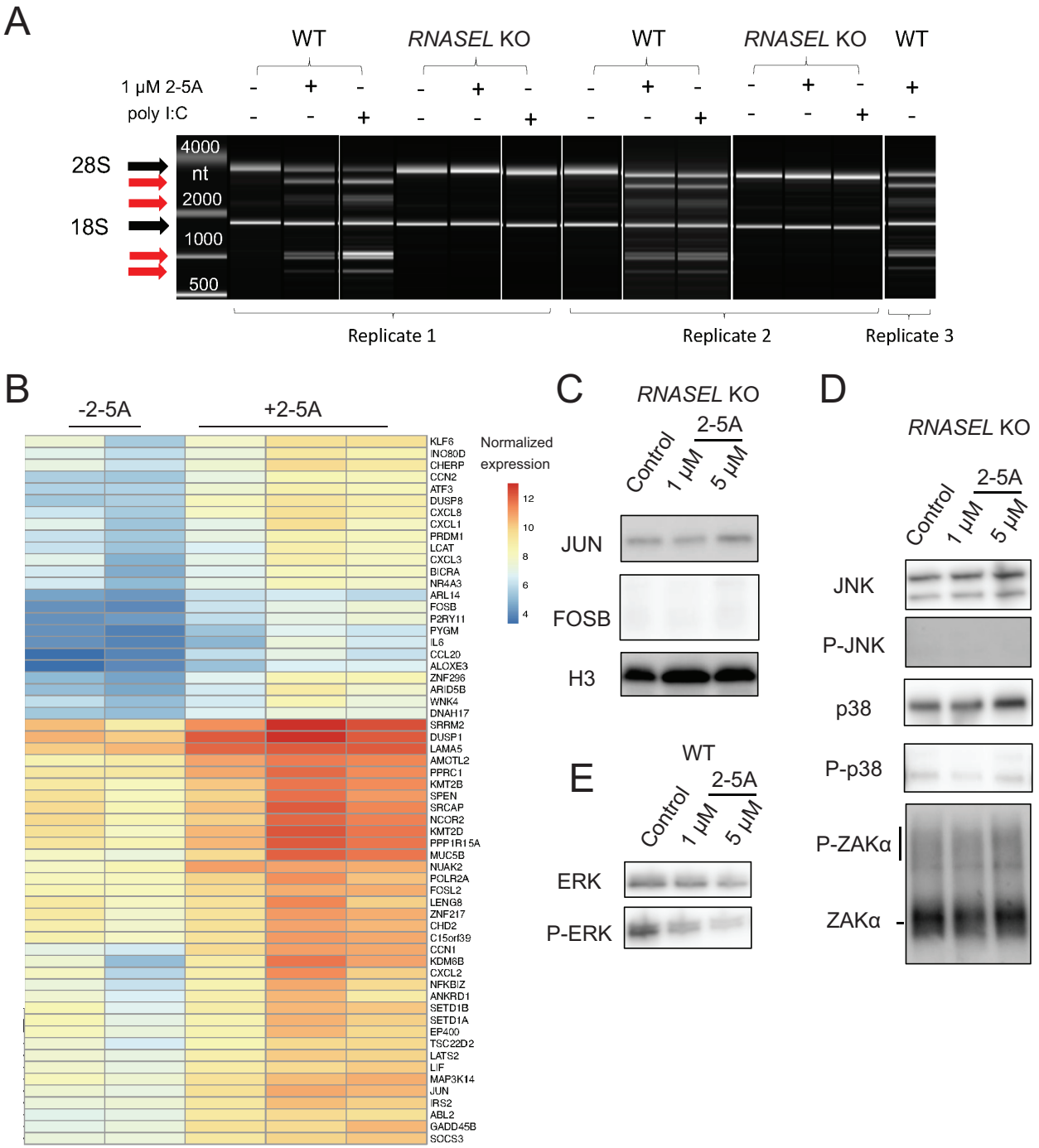
A
WT
RNASEL KO
WT
RNASEL KO
WT
1 μM 2-5A
poly I:C
28S
18S
4000
nt
2000
1000
500
Replicate 1
Replicate 2
Replicate 3
B
-2-5A
+2-5A
Normalized expression
12
10
8
6
4
KLF6
INO80D
CHERP
CCN2
ATF3
DUSP8
CXCL8
CXCL1
PRDM1
LCAT
CXCL3
BICRA
NR4A3
ARL14
FOSB
P2RY11
PYGM
IL6
CCL20
ALOXE3
ZNF296
ARID5B
WNK4
DNAH17
SRRM2
DUSP1
LAMA5
AMOTL2
PPRC1
KMT2B
SPEN
SRCAP
NCOR2
KMT2D
PPP1R15A
MUC5B
NUAK2
POLR2A
FOSL2
LENG8
ZNF217
CHD2
C15orf39
CCN1
KDM6B
CXCL2
NFKBIZ
ANKRD1
SETD1B
SETD1A
EP400
TSC22D2
LATS2
LIF
MAP3K14
JUN
IRS2
ABL2
GADD45B
SOCS3
C
RNASEL KO
2-5A
Control
1 μM
5 μM
JUN
FOSB
H3
E
WT
2-5A
Control
1 μM
5 μM
ERK
P-ERK
D
RNASEL KO
2-5A
Control
1 μM
5 μM
JNK
P-JNK
p38
P-p38
P-ZAKα
ZAKα

Figure S2

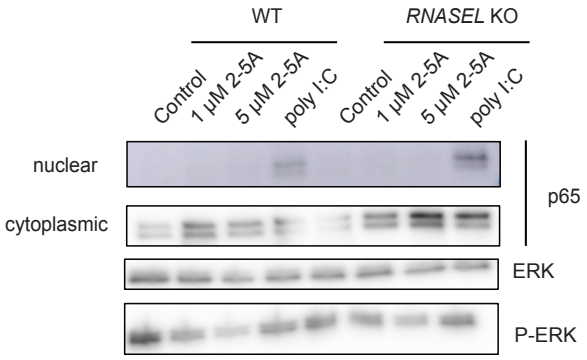
WT
RNASEL KO
Control
1 μM 2-5A
5 μM 2-5A
poly I:C
Control
1 μM 2-5A
5 μM 2-5A
poly I:C
nuclear
cytoplasmic
p65
ERK
P-ERK

Figure S3

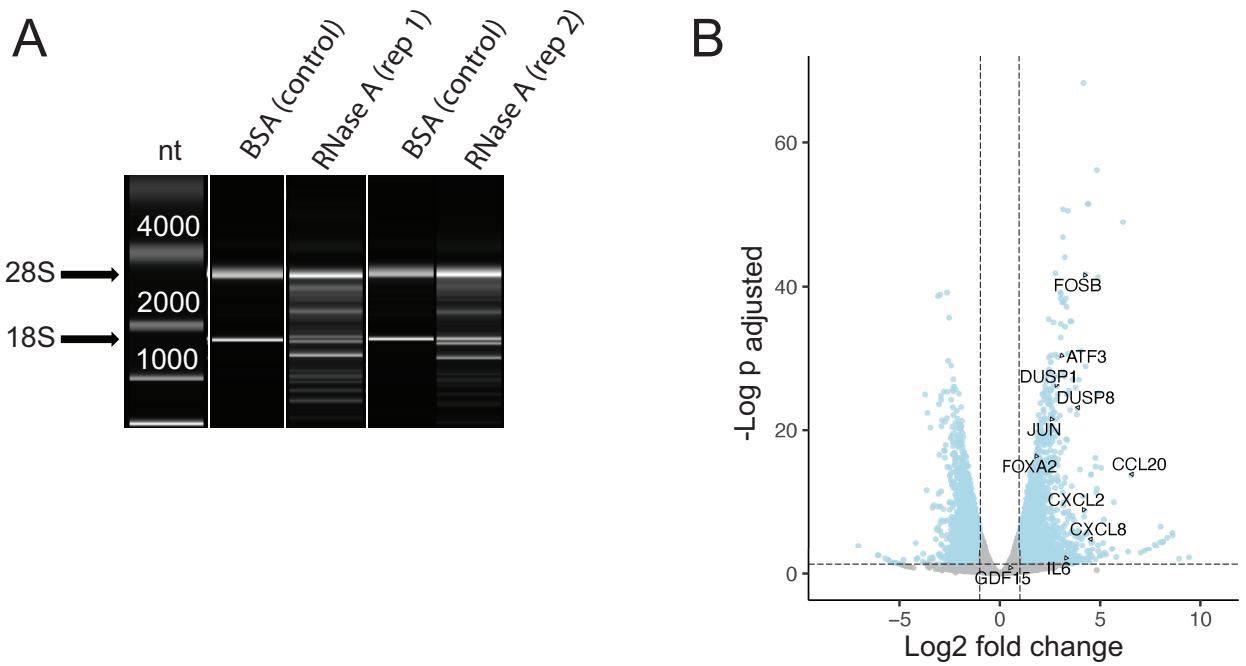
A
nt
BSA (control)
RNase A (rep 1)
BSA (control)
RNase A (rep 2)
4000
2000
1000
28S
18S
B
-Log p adjusted
Log2 fold change
FOSB
ATF3
DUSP1
DUSP8
JUN
FOXA2
CCL20
CXCL2
CXCL8
IL6
GDF15

Figure S4

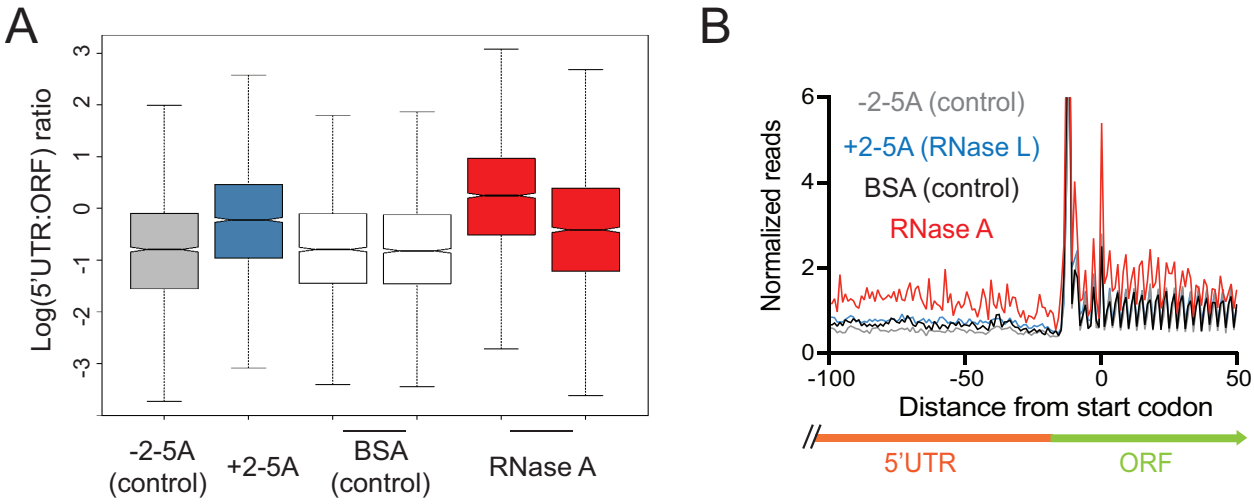
A
Log(5'UTR:ORF) ratio
3
2
1
0
-1
-2
-3
-2-5A (control)
+2-5A
BSA (control)
RNase A
B
Normalized reads
6
4
2
0
-2-5A (control)
+2-5A (RNase L)
BSA (control)
RNase A
-100
-50
0
50
Distance from start codon
5'UTR
ORF

Figure S5

A

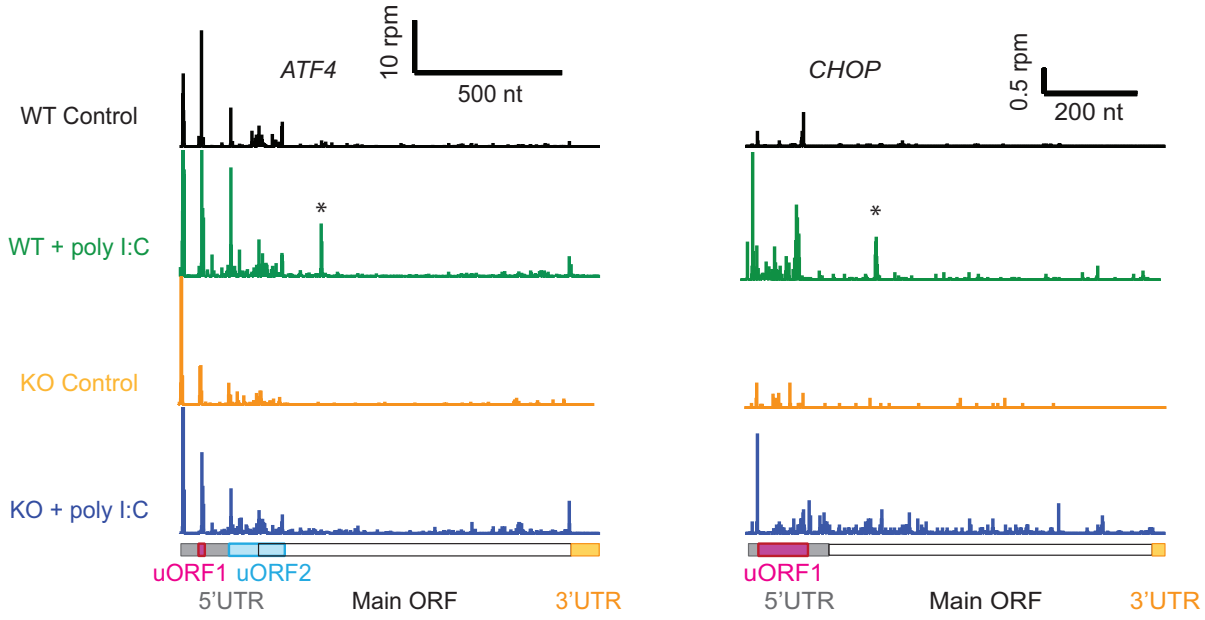
ATF4
10 rpm
500 nt
CHOP
0.5 rpm
200 nt
WT Control
WT + poly I:C
KO Control
KO + poly I:C
*
*
uORF1
uORF2
5'UTR
Main ORF
3'UTR
uORF1
5'UTR
Main ORF
3'UTR

B

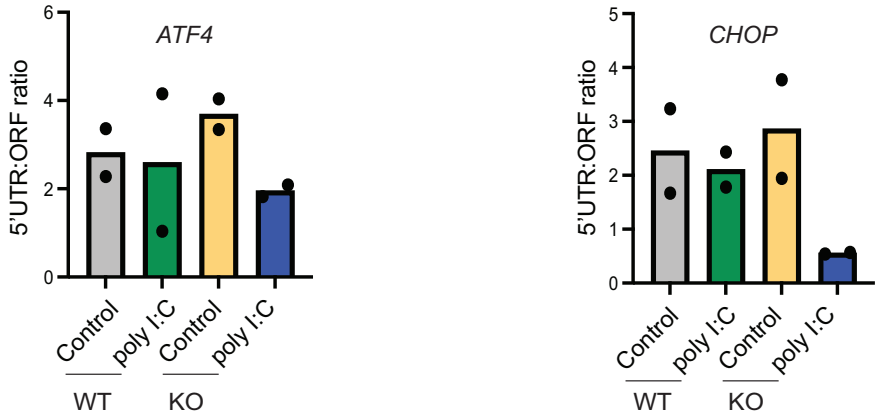
ATF4
5'UTR:ORF ratio
0
2
4
6
Control
poly I:C
Control
poly I:C
WT
KO
CHOP
5'UTR:ORF ratio
0
1
2
3
4
5
Control
poly I:C
Control
poly I:C
WT
KO

Figure S6

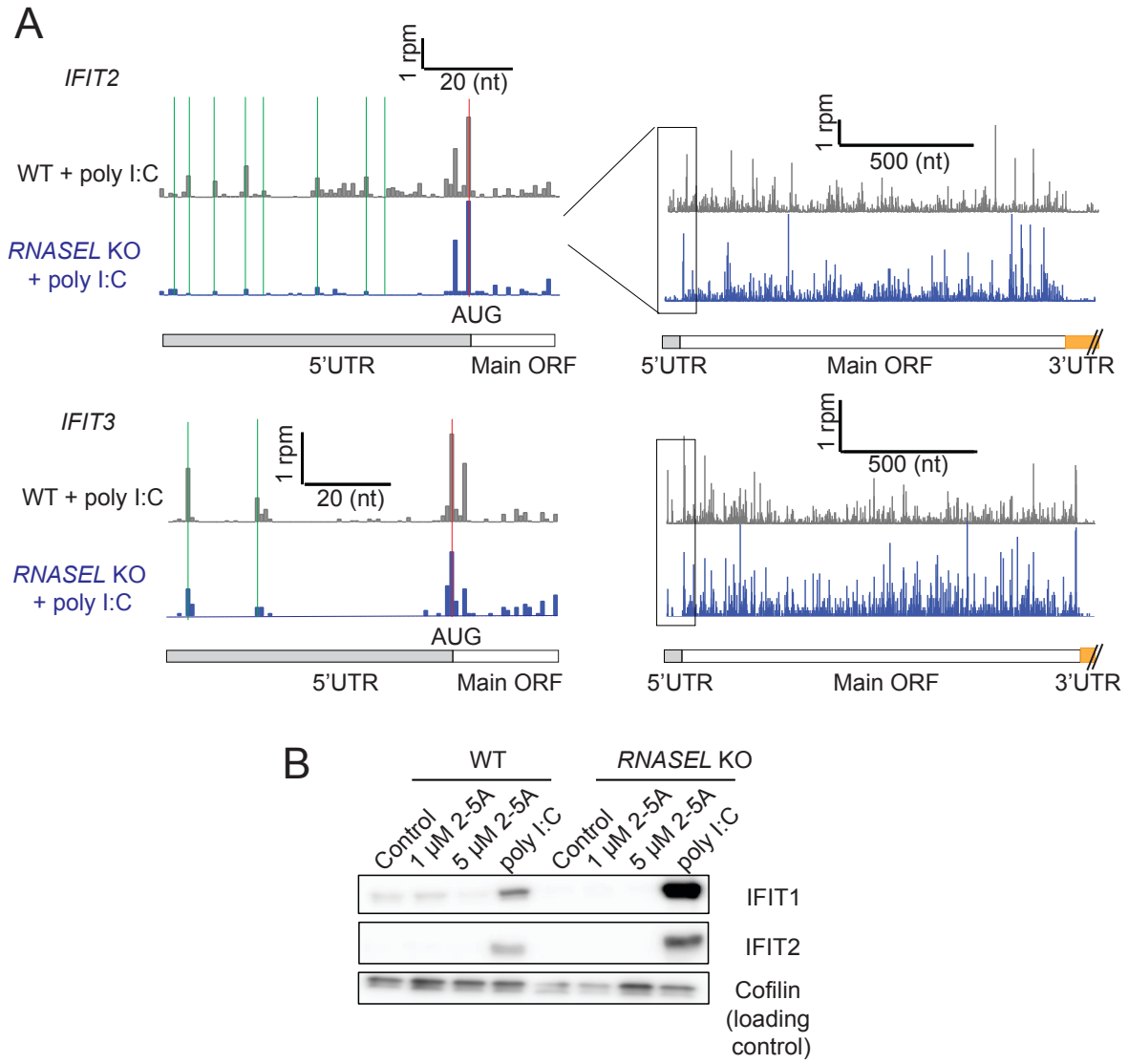
A
IFIT2
1 rpm
20 (nt)
WT + poly I:C
RNASEL KO
+ poly I:C
AUG
5'UTR
Main ORF
1 rpm
500 (nt)
5'UTR
Main ORF
3'UTR
IFIT3
1 rpm
20 (nt)
WT + poly I:C
RNASEL KO
+ poly I:C
AUG
5'UTR
Main ORF
1 rpm
500 (nt)
5'UTR
Main ORF
3'UTR
B
WT
RNASEL KO
Control
1 μM 2-5A
5 μM 2-5A
poly I:C
Control
1 μM 2-5A
5 μM 2-5A
poly I:C
IFIT1
IFIT2
Cofilin
(loading
control)